



Kent Academic Repository

Vasilopoulou, Elisavet, Kolatsi-Joannou, Maria, Lindenmeyer, Maja T, White, Kathryn E, Robson, Michael G, Cohen, Clemens D, Sebire, Neil J, Riley, Paul R, Winyard, Paul J and Long, David A (2016) *Loss of endogenous thymosin β 4 accelerates glomerular disease*. *Kidney international*, 90 (5). pp. 1056-1070. ISSN 0085-2538.

Downloaded from

<https://kar.kent.ac.uk/63429/> The University of Kent's Academic Repository KAR

The version of record is available from

<https://doi.org/10.1016/j.kint.2016.06.032>

This document version

Author's Accepted Manuscript

DOI for this version

Licence for this version

CC BY-NC-ND (Attribution-NonCommercial-NoDerivatives)

Additional information

Versions of research works

Versions of Record

If this version is the version of record, it is the same as the published version available on the publisher's web site. Cite as the published version.

Author Accepted Manuscripts

If this document is identified as the Author Accepted Manuscript it is the version after peer review but before type setting, copy editing or publisher branding. Cite as Surname, Initial. (Year) 'Title of article'. To be published in **Title of Journal**, Volume and issue numbers [peer-reviewed accepted version]. Available at: DOI or URL (Accessed: date).

Enquiries

If you have questions about this document contact ResearchSupport@kent.ac.uk. Please include the URL of the record in KAR. If you believe that your, or a third party's rights have been compromised through this document please see our [Take Down policy](https://www.kent.ac.uk/guides/kar-the-kent-academic-repository#policies) (available from <https://www.kent.ac.uk/guides/kar-the-kent-academic-repository#policies>).

Revised version of KI-10-15-1651

Loss of endogenous thymosin- β 4 accelerates glomerular disease

Elisavet Vasilopoulou¹, Maria Kolatsi-Joannou¹, Maja T Lindenmeyer², Kathryn E White³,
Michael G Robson⁴, Clemens D Cohen², Neil J Sebire¹, Paul R Riley⁵, Paul J Winyard¹,
David A Long¹

¹Developmental Biology and Cancer Programme, UCL Institute of Child Health, London,
WC1N 1EH, UK

²Nephrological Center, Medical Clinic and Policlinic IV, University of Munich, Munich,
Germany

³EM Research Services, University of Newcastle, Newcastle upon Tyne, NE2 4HH, UK

⁴MRC Centre for Transplantation, King's College London, London, SE1 9RT, UK

⁵Department of Physiology, Anatomy and Genetics, University of Oxford, Oxford, OX1 3PT,
UK

Corresponding Author

David A Long PhD, Developmental Biology and Cancer Programme,
UCL Institute of Child Health, 30 Guilford Street, London, WC1N 1EH, UK

Tel: +44 (0)207 905 2615

Fax: +44 (0)207 905 2133;

E-mail: d.long@ucl.ac.uk

Word Count: Abstract 165, Text: 4431

Running Title: Thymosin- β 4 and glomerular disease

ABSTRACT

Glomerular disease is characterised by morphological changes in podocyte cells accompanied by inflammation and fibrosis. Thymosin- β 4 regulates cell morphology, inflammation and fibrosis in several organs and administration of exogenous thymosin- β 4 improves animal models of unilateral ureteral obstruction and diabetic nephropathy. However, the role of endogenous thymosin- β 4 in the kidney is unknown. We demonstrate thymosin- β 4 is expressed prominently in podocytes of developing and adult mouse glomeruli. Global loss of thymosin- β 4 did not affect healthy glomeruli, but accelerated the severity of immune-mediated nephrotoxic nephritis with worse renal function, peri-glomerular inflammation and fibrosis. Lack of thymosin- β 4 in nephrotoxic nephritis led to the redistribution of podocytes from the glomerular tuft towards the Bowman's capsule suggesting a role for thymosin- β 4 in the migration of these cells. Thymosin- β 4 knock-down in cultured podocytes also increased migration in a wound-healing assay; accompanied by F-actin rearrangement and increased RhoA activity. We propose that endogenous thymosin- β 4 is a modifier of glomerular injury, likely having a protective role acting as a brake to slow disease progression.

Keywords: cytoskeleton, fibrosis, glomerulus, inflammation, podocyte

INTRODUCTION

End-stage renal failure is a devastating condition, requiring life-long dialysis and transplantation and a risk factor for all-cause mortality and cardiovascular disease.¹ Many cases are due to disruption of the glomerular filtration barrier, consisting of epithelial podocytes, endothelium, mesangium and glomerular basement membrane.² Podocytes have a unique shape maintained by a complex cytoskeleton,³ with branched foot process extensions which abut each other at slit diaphragms. During glomerular injury, podocyte architecture is perturbed resulting in defective filtration and proteinuria²⁻⁴ often with inflammatory components characterised by leukocyte infiltration followed by glomerulosclerosis and tubulointerstitial fibrosis.⁵

Thymosin- β 4 (Tmsbx4) is a naturally-occurring peptide. It is the major G-actin sequestering protein in mammalian cells⁶ with critical roles in maintaining the cell cytoskeleton. In animal models, exogenous Tmsbx4 has beneficial effects in diverse pathologies including myocardial infarction,⁷ stroke,⁸ dry eye⁹ and inflammatory lung disease;¹⁰ and there are clinical trials assessing Tmsbx4 treatment in wound healing and cardioprotection.¹¹ The utility of Tmsbx4 in these pathologies has been attributed to modulation of several cellular functions including cell motility,¹² differentiation,¹³ survival,¹⁴ angiogenesis,¹⁵ inflammation¹⁶ and fibrosis.¹⁰

Recent studies investigated exogenous Tmsbx4 as a treatment for kidney disease.¹⁷ Tmsbx4 reduced renal tubulointerstitial fibrosis following unilateral ureteral obstruction (UUO) in mice, potentially through decreasing plasminogen activator inhibitor-1 (PAI-1) expression and dampening transforming growth factor- β 1 signalling.¹⁸ In *KK Cg-Ay/J* mice, a model of type II diabetes mellitus, daily Tmsbx4 treatment for three months reduced albuminuria and attenuated renal pathology.¹⁹ Furthermore, N-acetyl-seryl-aspartyl-lysyl-proline (AcSDKP), the N-terminal tetrapeptide generated by Tmsbx4 cleavage²⁰ has

beneficial effects on fibrosis and inflammation in UUO, remnant kidneys, diabetic nephropathy and glomerulonephritis.^{18, 21-23}

Tmsbx4 transcripts are detectable by *in-situ* hybridisation in developing and adult glomeruli²⁴ with strong expression in podocytes.^{24, 25} Furthermore, in rat remnant kidneys, proteomic analysis of laser-capture dissected glomeruli demonstrated significantly increased *Tmsbx4* in sclerotic *versus* normal glomeruli.²⁶ Despite such evidence of expression and beneficial renal effects, the functional importance of endogenous *Tmsbx4* in the kidney during health and disease is completely unknown.

In this study, we confirmed *Tmsbx4* is highly expressed in the kidney glomerulus, predominately in podocytes. Using global *Tmsbx4* knock-out mice²⁷ we demonstrated that endogenous *Tmsbx4* was dispensable in healthy glomeruli. Furthermore, in an experimental model of glomerular damage, lack of *Tmsbx4* worsened disease progression by (i) enhancing podocyte migration facilitating their redistribution from glomerular tuft to Bowman's capsule, and (ii) increasing peri-glomerular inflammation and interstitial fibrosis. Thus we provide the first evidence that endogenous *Tmsbx4* is critical in the progression of glomerular disease.

RESULTS

Tmsb4x is expressed in mouse glomerular podocytes

Tmsb4x mRNA levels were assessed in spleen, liver, heart and the whole kidney of healthy adult mice. The highest transcript levels were found in the spleen with approximately 10 times less *Tmsb4x* in the kidney (**Figure 1A**). Using Dynabead perfusion²⁸ we isolated glomeruli and found *Tmsb4x* levels were significantly enriched in glomeruli compared with the rest of the kidney (**Figure 1A**). *In-situ* hybridisation detected *Tmsb4x* expression in immature glomeruli of embryonic day (E)16.5 developing kidneys, predominately in podocytes (**Figure 1B-C**). The protein expression of *Tmsb4x* was also assessed by immunohistochemistry and we found strong localisation in glomerular podocytes at E18 (**Figure 1D**). This expression pattern was maintained in one-week-old postnatal (**Figure 1E**) and eight-week-old adult kidneys (**Figure 1F**). *Tmsb4x* podocyte expression was further confirmed by co-localisation of *Tmsb4x* with nephrin (*Nphs1*), a slit diaphragm component²⁹ (**Figure 1G-I**) and nestin, an intermediate filament protein expressed in mature podocytes³⁰ (**Supplementary Figure 1A-C**). In contrast, *Tmsbx4* did not co-localise with the pan-endothelial marker, Cd31 (**Supplementary Figure 1D-F**).

Lack of endogenous *Tmsb4x* has no effect on healthy glomeruli

We examined mice with a global loss of *Tmsb4x*²⁷ to assess the importance of endogenous *Tmsb4x* in healthy glomeruli. As *Tmsb4x* is mapped to the X chromosome,³¹ we crossed hemizygous null male mice (*Tmsb4x*^{-y}) with heterozygous *Tmsb4x*^{+/-} adult females (**Figure 2A**). We found no lethal developmental abnormalities with the offspring conforming to Mendelian ratios (**Supplementary Table 1**). *Tmsb4x*^{-y} mice had similar albumin excretion (**Figure 2B**) and blood urea nitrogen (BUN) levels (**Figure 2C**) as male wild-type *Tmsb4x*^{+y} mice at the ages of 1, 3 and 6 months. There was no difference in body weight at 1 (*Tmsb4x*^{+y}=23.8±0.7g; *Tmsb4x*^{-y}=23.4±0.4g), 3 (*Tmsb4x*^{+y}=30.0±0.5g; *Tmsb4x*^{-y}=29.2±0.7g), or 6 months of age (*Tmsb4x*^{+y}=35.8±1.0g; *Tmsb4x*^{-y}=35.3±1.6g). Using semi-quantitative analysis of light microscopy images, we found no differences in glomerular

morphology between six-month-old *Tmsb4x^{+/-}* and *Tmsb4x^{-/-}* mice (**Figure 2D-F**). This was confirmed by transmission electron microscopy with normal foot process architecture, laminar structure of the basement membrane and the presence of endothelial fenestrae in both *Tmsb4x^{+/-}* and *Tmsb4x^{-/-}* mice (**Figure 2G-H**). We demonstrated the loss of Tmsb4x protein in glomeruli of *Tmsb4x^{-/-}* mice compared with *Tmsb4x^{+/-}* (**Figure 2I-J**); along with undetectable *Tmsb4x* mRNA levels in whole kidneys (**Figure 2K**). We examined whether there was any compensation for the lack of *Tmsb4x* by other β -thymosins, but found no changes in the renal mRNA levels of *Tmsb10*, *Tmsb15a*, *Tmsb15b* and *Tmsb15l* (**Figure 2L-O**). We also assessed mRNA levels of genes involved in actin polymerisation and found no differences in profilin (*Pfn*)-1 and -2 and destrin (*Dstn*) between *Tmsb4x^{-/-}* and *Tmsb4x^{+/-}* mice (**Supplementary Figure 2A-C**). In contrast, cofilin 1 (*Cfl1*) mRNA levels were significantly increased in *Tmsb4x^{-/-}* kidneys by approximately 30% compared with *Tmsb4x^{+/-}* mice (**Supplementary Figure 2D**). We specifically examined *Cfl1* mRNA levels in podocytes and found no change following knockdown of endogenous *Tmsb4x* by small interfering RNA (siRNA) (**Supplementary Figure 2E**). Furthermore, there was no difference in *Cfl1* mRNA levels in primary podocytes isolated from *Tmsb4x^{-/-}* and *Tmsb4x^{+/-}* mice (**Supplementary Figure 2F**). Finally, the mRNA levels of genes important for podocyte function, (*Nphs1*, *Nphs2*, *Synpo*, *Cd2ap* and *Wt1*) were unchanged between *Tmsb4x^{-/-}* and *Tmsb4x^{+/-}* kidneys (**Supplementary Figure 3A-E**).

Lack of endogenous *Tmsbx4* worsens renal function and glomerular injury in NTS nephritis

Our results suggest lack of *Tmsbx4* does not affect the function and morphology of healthy glomeruli. Therefore, we investigated whether *Tmsbx4* has a role in glomerular disease. We utilised the NTS nephritis model, which replicates some of the pathological features of human crescentic glomerulonephritis.³² NTS nephritis involves the injury of intrinsic glomerular cells, including podocytes, as well as leukocyte infiltration, glomerulosclerosis and tubulointerstitial fibrosis,³³ processes in which *Tmsbx4* has been implicated.^{10, 16} We

predicted that lack of global *Tmsbx4* may exacerbate NTS nephritis severity and examined this in three month old *Tmsb4x^{-/y}* and *Tmsb4x^{+/y}* mice (**Figure 3A**). Albuminuria and albumin/creatinine ratio was significantly increased in *Tmsb4x^{+/y}* mice twenty-one days after NTS administration compared with the levels prior to immunisation ($p < 0.001$ in both cases, **Figure 3B-C**). Strikingly, both albuminuria and albumin/creatinine ratio was further enhanced by approximately 5- and 7-fold respectively when NTS was injected to *Tmsb4x^{-/y}* compared with *Tmsb4x^{+/y}* mice ($p < 0.01$ in both cases, **Figure 3B-C**). Administration of NTS to *Tmsb4x^{-/y}* mice also significantly elevated plasma creatinine ($p < 0.01$, **Figure 3D**), impaired creatinine clearance ($p < 0.01$; **Figure 3E**) and raised BUN ($p < 0.05$, **Figure 3F**) compared with *Tmsb4x^{+/y}* mice with nephrotoxic nephritis. We found no difference in *Tmsb4x* levels in whole kidneys obtained from *Tmsb4x^{+/y}* mice without disease or administered NTS (**Supplementary Figure 4A**). Furthermore, in kidney biopsies obtained from patients with either rapidly progressive glomerulonephritis (RPGN) or lupus nephritis (SLE), there was no change in glomerular or tubulointerstitial *TMSB4X* mRNA levels compared with living donor (LD) control kidneys (**Supplementary Figure 4B-C**).

Seven days after NTS administration, we observed mild glomerular injury in *Tmsb4x^{-/y}* and *Tmsb4x^{+/y}* mice with some glomeruli containing hyaline deposits, increased mesangial matrix and occasional adhesion of the glomerular tuft to Bowman's capsule (**Supplementary Figure 5A-C**). After twenty-one days, there was a range of abnormalities in *Tmsb4x^{-/y}* and *Tmsb4x^{+/y}* mice injected with NTS including collapse of capillary loops, segmental or global glomerulosclerosis, adhesion of the tuft to Bowman's capsule and glomerular epithelial hyperplasia lesions, a feature of early crescent formation in this model.³⁴ Semi-quantitative histological scoring (**Supplementary Figure 6A-E**) by two blinded observers revealed that *Tmsb4x^{+/y}* mice injected with NTS had significantly raised mean glomerular score compared with *Tmsb4x^{+/y}* mice without disease ($p < 0.001$, **Figure 3G-J**). Glomeruli of *Tmsb4x^{-/y}* administered NTS had an even higher glomerular mean score which was significantly greater than *Tmsb4x^{+/y}* mice with nephrotoxic nephritis ($p < 0.05$). This was associated with

an increased proportion of sclerotic glomeruli and incidence of epithelial hyperplasia lesions in *Tmsb4x^{-/-}* compared with *Tmsb4x^{+/-}* mice administered NTS (**Supplementary Figure 6F**).

We examined whether the difference in disease severity between *Tmsb4x^{-/-}* and *Tmsb4x^{+/-}* mice with NTS could be due to a decrease in binding of the anti-glomerular antibody but found no difference in the amount of sheep IgG deposited within the glomerulus (**Supplementary Figure 7A-C**). We assessed whether lack of *Tmsbx4* changes the humoral immune response to sheep IgG. NTS injection led to significantly increased production of circulating murine IgG1 and IgG2a, but not IgG2b or IgG3 against sheep IgG compared with *Tmsb4x^{+/-}* mice without disease. However there was no difference in the plasma titres of any of the IgG subclasses between *Tmsb4x^{-/-}* and *Tmsb4x^{+/-}* mice administered NTS (**Supplementary Figure 7D-G**).

Changes in podocyte distribution in *Tmsb4x^{-/-}* glomeruli following NTS nephritis

Following NTS nephritis, we found that *Tmsbx4* still co-localised with *Nphs1* (**Figure 4A-C**) and subsequently examined the effect a lack of *Tmsbx4* had on podocytes in this model. Firstly, we quantified *WT1⁺* podocyte numbers,³⁵ in and outside of the glomerular tuft (**Figure 4D-F**). The number of glomerular tuft *WT1⁺* cells was unchanged in *Tmsb4x^{+/-}* mice following NTS injection compared with mice without disease. However, NTS administration to *Tmsb4x^{-/-}* mice significantly reduced the number of *WT1⁺* glomerular tuft cells compared with *Tmsb4x^{+/-}* mice with nephrotoxic nephritis ($p < 0.001$; **Figure 4G**). This finding persisted after normalising the *WT1⁺* cell number to glomerular tuft area ($p < 0.05$; **Figure 4H**). In contrast, there was an increased number of *WT1⁺* cells outside the glomerular tuft in both *Tmsb4x^{+/-}* and *Tmsb4x^{-/-}* mice following NTS administration, this was more prominent and significantly different in the *Tmsb4x^{-/-}* animals ($p < 0.05$ compared with *Tmsb4x^{+/-}* without disease; **Figure 4I**). The total number of podocytes in the whole glomerulus did not differ between any of the groups (**Figure 4J**), suggesting that lack of *Tmsb4x* leads to podocyte redistribution from the glomerular tuft towards the Bowman's capsule rather than affecting podocyte cell death. To

support this, we assessed podocyte apoptosis using terminal deoxynucleotidyl transferase dUTP nick end labeling (TUNEL)³⁶ in combination with WT1 staining (**Supplementary Figure 8A-C**). Administration of NTS increased the number of glomerular apoptotic cells compared with healthy mice and this effect was significant in *Tmsb4x*^{+/-} mice with glomerular disease ($p < 0.05$; **Supplementary Figure 8D**). However, the number of TUNEL⁺/WT1⁺ cells was not significantly different between any of the groups (**Supplementary Figure 8E**).

Lack of *Tmsb4x* induces migration and modulates the cytoskeleton of podocytes *in vitro*

We postulated that the redistribution of podocytes in nephrotoxic nephritis may be due to changes in cell migration driven by lack of *Tmsb4x*. Therefore, we transfected cultured differentiated mouse podocytes³⁷ with siRNA against *Tmsb4x* (**Figure 5A**): this resulted in >90% knockdown in *Tmsb4x* levels (**Figure 5B**; $p < 0.001$). Knockdown of endogenous *Tmsb4x* did not affect podocyte viability (**Figure 5C**) but increased the number of cells that migrated into the wound area in a wound-healing assay ($p < 0.05$; **Figure 5D-E**). Since the cytoskeleton is essential for cell movement,³⁸ we visualised podocyte actin by phalloidin staining and classified the filament organisation as either cytoplasmic stress fibres (**Figure 5F**) or cortical actin (**Figure 5G**). Knockdown of endogenous *Tmsb4x* significantly increased the percentage of cells with stress actin fibre organisation ($p < 0.001$; **Figure 5H**). Finally, we assessed the effects of *Tmsb4x* knockdown on the activation of RhoA and Cdc42, which regulate actin dynamics and cell migration.³⁹ There was increased RhoA activity in podocytes transfected with *Tmsb4x* siRNA compared to control siRNA ($p < 0.05$; **Figure 5I**) whereas Cdc42 activity was unaffected (**Figure 5J**).

Macrophage accumulation and increased fibrosis in *Tmsb4x*^{-/-} glomeruli following NTS nephritis

Tmsb4x is expressed in macrophages^{18, 40} and reduces inflammation in several disease settings.^{10, 16, 18, 41} As immune cell infiltration plays a critical role in the initiation and

progression of crescentic glomerulonephritis.⁴²⁻⁴⁴ We found expression of *Tmsb4x* in F4/80⁺ macrophages surrounding the glomeruli and occasionally within the glomerular tuft (**Figure 6A-C**) and went on to examine the effect of *Tmsb4x* loss on glomerular inflammation in our experimental model.

We measured the number of Cd3⁺ (T cells) and F4/80⁺ cells in *Tmsb4x*^{-/-} and *Tmsb4x*^{+/-} glomeruli. Twenty-one days after NTS injection there was a significant increase in Cd3⁺ cells in the glomerular tuft of *Tmsb4x*^{-/-} mice compared with *Tmsb4x*^{+/-} without disease ($p < 0.05$) but no significant difference when comparing *Tmsb4x*^{-/-} and *Tmsb4x*^{+/-} mice with nephrotoxic nephritis (**Figure 6D-G**). There was also no difference in the number of peri-glomerular Cd3⁺ cells between experimental groups (**Figure 6H**). Seven days following NTS administration, the number of F4/80⁺ glomerular tuft cells was similar in all experimental groups, but were significantly elevated in the peri-glomerular area of both NTS-injected *Tmsb4x*^{+/-} and *Tmsb4x*^{-/-} mice compared with healthy mice ($p < 0.01$; **Supplementary Figure 9A-B**). The accumulation of F4/80⁺ cells persisted in *Tmsb4x*^{-/-} mice twenty-one days after NTS administration, with increased numbers in both the glomerular tuft and peri-glomerular area compared with *Tmsb4x*^{+/-} mice with or without disease ($p < 0.01$, **Figure 6I-M**). mRNA levels of the pan-macrophage marker, *Cd68*, were also significantly higher twenty-one days following NTS injection in whole kidney homogenates obtained from *Tmsb4x*^{-/-} compared with *Tmsb4x*^{+/-} mice (**Supplementary Figure 10A**). *Cd68* is expressed by all macrophages, but these comprise a diverse group which includes a broad spectrum of cellular phenotypes, often characterised as pro-inflammatory (M1-type) and tissue repair (M2-type) macrophages. We quantified the mRNA levels of M1 (*Mcp1*, *Cd86*) and M2 markers (*Cd206*, *Arg1*) and found all of these genes were significantly upregulated in *Tmsb4x*^{-/-} mice compared with *Tmsb4x*^{+/-} following NTS (**Supplementary Figure 10B-E**). This suggests that there is a global increase in macrophages in *Tmsb4x*^{-/-} kidneys following NTS rather than a shift towards a M1 or M2 phenotype.

Finally, the increased accumulation of macrophages in the peri-glomerular area in *Tmsb4x^{-/y}* mice with NTS was associated with increased peri-glomerular fibrosis as shown by increased staining for both collagen IV (**Figure 7A-C**) and alpha smooth muscle actin (α -SMA) (**Figure 7E-G**) in sections from *Tmsb4x^{-/y}* compared with *Tmsb4x^{+/y}* mice injected with NTS along with increased whole kidney mRNA levels of *Col4a1* ($p < 0.05$; **Figure 7D**) and *Acta2* ($p < 0.05$; **Figure 7H**).

DISCUSSION

In this study we found endogenous *Tmsbx4* was not required to maintain glomerular structure and function in healthy adult mice. However, in an experimental model of NTS nephritis, glomerular disease was exacerbated in mice lacking *Tmsbx4* accompanied by changes in the distribution of podocytes within the glomerulus, increased peri-glomerular macrophage accumulation and enhanced fibrosis. These findings provide the first evidence that endogenous *Tmsbx4* modifies glomerular injury, likely having a protective role acting as a brake to slow disease progression.

We showed that *Tmsbx4* is expressed in developing and adult mouse glomeruli, predominantly localised to podocytes. Prior studies have also found *Tmsbx4* in glomerular podocytes,²⁵ but others have reported complete absence of *Tmsbx4* in the glomeruli of human fetal and adult kidneys⁴⁵ and rat kidneys.²⁶ These discrepancies may be due to differences in the antibodies and fixation methods used.⁴⁶ Importantly, we obtained similar results for both *Tmsb4x* mRNA and protein and confirmed the specificity of antibody staining using tissues from *Tmsb4x*^{-/-} mice as an additional negative control.

Given that *Tmsbx4* plays a role in actin binding,⁶ we initially hypothesised that lack of endogenous *Tmsbx4* might disrupt the highly-branched architecture of glomerular podocytes and impair renal function.³ However, lack of *Tmsbx4* did not affect glomerular morphology or podocyte architecture of normal healthy mice *in-vivo*. We found upregulation of *Cfn1*, which severs actin filaments, in whole *Tmsb4x*^{-/-} kidneys. This could partly compensate for the lack of *Tmsb4x* and maintain actin dynamics,⁴⁷ however, *Cfn1* was not specifically altered in podocytes lacking *Tmsb4x* thus making this unlikely.

A significant finding of our study was that severity of glomerular disease induced by NTS was greater in *Tmsb4x*^{-/-} mice compared with wild-type littermates. We postulate endogenous *Tmsb4x* has a protective role in the setting of NTS, a prediction supported by a

study showing exogenous administration of Ac-SDKP ameliorated rat glomerulonephritis.²² However, we found whole mouse kidney *Tmsb4x* mRNA levels were unchanged with NTS nephritis and this was mirrored when we assessed *TMSB4X* mRNA levels in glomerular and tubulointerstitial extracts from human kidneys affected by RPGN or SLE. In contrast, a previous study in rat remnant kidneys where nephron loss results in focal segmental glomerulosclerosis showed *Tmsbx4* protein levels were significantly increased in sclerotic *versus* normal glomeruli.²⁶ The discrepancy between these findings may be due to the different renal injury models and time-points examined.

There are likely to be multiple mechanisms by which lack of endogenous *Tmsb4x* results in increased glomerular injury in our experimental model. During nephrotoxic nephritis, podocytes switch from a terminally-differentiated cell to a migratory cell that forms bridges between the glomerular tuft and the Bowman's capsule³⁴ and populates glomerular crescents.^{30, 48} Lack of *Tmsbx4* increased the number of glomeruli with adhesion of the tuft to the Bowman's capsule and glomerular epithelial hyperplasia lesions, a feature of early crescent formation in this model.³⁴ We also found there was a redistribution of podocytes from the glomerular tuft, where they contribute to filtration barrier integrity, towards the Bowman's capsule. Our *in-vitro* data demonstrates that downregulation of endogenous *Tmsbx4* in podocytes increases migration and we predict that this may promote their redistribution in the nephrotoxic nephritis model. The increased podocyte migration was associated with increased actin stress fibres and activation of RhoA, which has been linked to podocyte stress fibre formation.^{49, 50} Moreover, podocyte-specific overexpression of RhoA induces proteinuria^{50, 51} whereas RhoA inhibition improves renal injury in mouse models of nephrectomy⁵² and nephrotoxic nephritis⁵³, demonstrating the functional importance of this pathway in glomerular function. Other studies have shown RhoA activation inhibits podocyte migration,⁵⁴ but these experiments used a constitutively active form of RhoA permanently in the GTP-bound state. This would result in a high degree of RhoA activity which has been associated with inhibition of migration.⁵⁵ In contrast, *Tmsbx4* knockdown led to a 2-fold

upregulation of RhoA activity in podocytes. It has been postulated that this lesser degree of RhoA activation promotes contractile stress fibre formation facilitating cell detachment in migrating cells³⁹ and enhancing lamellipodia formation driving cell motility.⁵⁵ It has been previously reported that activation of other Rho GTPases, Cdc42 and Rac1, may increase podocyte migration.⁵⁶ However, we found that downregulation of endogenous *Tmsb4x* did not affect Cdc42 activation in podocytes. Rac1 activity was not assessed in this study and it would be interesting to explore its involvement in the future.

Tmsb4x is also expressed in macrophages,^{18, 40} including in our nephrotoxic nephritis model, but its precise function is yet to be determined. It could be postulated that loss of macrophage *Tmsbx4* may regulate the actin cytoskeleton which has been implicated in both phenotypic polarisation⁵⁷ and migration.⁵⁸ In our study, loss of *Tmsbx4* did not alter macrophage polarisation or the number of activated macrophages found in the glomerular area in the early stages of nephrotoxic nephritis. However the number of activated macrophages in the peri-glomerular area at the late stage of the disease was increased in *Tmsb4x*^{-/-} mice suggesting a deficiency in the resolution of inflammation resulting in persistent macrophage accumulation. Macrophage accumulation may result from an absence of the *Tmsb4x*-derivative thymosin- β 4-sulfoxide, which has been shown to disperse inflammatory macrophages at the injury site in zebrafish and mouse models of heart injury.⁵⁹ We also found that peri-glomerular fibrosis was enhanced in *Tmsb4x*^{-/-} mice following NTS administration compared with wild-type mice. This may represent a secondary effect of enhanced inflammation and glomerular damage. However, prior studies have shown that *Tmsbx4* can alter both PAI-1 and TGF- β 1,^{18, 27} both of which are drivers of fibrosis and play important roles in the progression of nephrotoxic nephritis.^{60, 61}

In summary, we have provided the first evidence that lack of endogenous *Tmsbx4* does not affect healthy glomeruli but exacerbates renal function impairment, peri-glomerular inflammation and fibrosis in the context of nephrotoxic nephritis. These findings suggest that

modulating Tmsbx4 could be a potential therapeutic target in immune-mediated glomerular disease.

METHODS

Experimental animals and procedures

C57Bl/6 hemizygous null male mice (*Tmsb4x^{-y}*) were bred with heterozygous *Tmsb4x^{+/-}* adult females to generate male wild-type (*Tmsb4x^{+y}*) and null mice.²⁷ For the induction of glomerular disease *Tmsb4^{+y}* and *Tmsb4x^{-y}* mice were pre-immunised by subcutaneous injection of sheep IgG (250µg) in complete Freund's adjuvant, followed by intravenous administration of sheep NTS (250µl) five days later.⁶² All procedures were approved by the UK Home Office.

Renal function

Urine was collected from mice by housing them individually in metabolic cages. Blood samples were collected from the lateral saphenous vein. Albumin concentrations were measured by enzyme-linked immunosorbent assay^{28, 63} (Bethyl Laboratories, Montgomery, TX). Urinary and plasma creatinine concentration was measured using isotope dilution electrospray mass spectrometry.⁶⁴ Creatinine clearance (µl/min per g of body weight) was derived from the formula $\text{urinary creatinine} \times \text{urine volume} \times 1440 \text{ min}^{-1} \times \text{plasma creatinine}^{-1} \times \text{body weight (g)}^{-1}$.⁶³ BUN was assessed using a commercially available assay kit, validated in mice (BioAssay Systems, Hayward, CA).⁶⁵

Histological Analysis and Immunohistochemistry

Kidneys were fixed in 4% paraformaldehyde, embedded in paraffin, 5µm sections cut and stained with periodic acid–Schiff reagent. 50 glomeruli/sample were scored by two blinded observers using the following system: 0=normal glomerular structure; 1=increased mesangial matrix deposition and hypercellularity, some loss of capillary loops; 2=increased matrix deposition and focal areas of sclerosis; 3=>50% of glomerulus sclerotic, very few capillary loops; 4=>75% of glomerulus sclerotic and presence of glomerular epithelial hyperplasia lesions (**Supplementary Figure 5**). An average score was obtained for each kidney.

Immunohistochemistry or immunofluorescence was performed⁶⁶ using antibodies against *Tmsb4x* (A9520, Immundiagnostik, Bensheim, Germany), Collagen IV (ab19808, Abcam, Cambridge, UK), Cd3 (ab16669, Abcam), α -SMA (M0851, Dako, Ely, UK), F4/80 (MCA497R, AbD Serotec, Oxford, UK), Nphs1 (GP-N2, Progen, Heidelberg, Germany), Nestin (NB100-1604, Novus Biologicals, Littleton, CO), WT1 (AP15857PU-S, Acris Antibodies, Herford, Germany), Cd31 (MA3105, Thermo Fisher Scientific, Waltham, MA) and Sheep IgG (A11016, Thermo Fisher Scientific). CD3⁺ and F4/80⁺ cells were counted in 50 glomeruli/sample. To assess glomerular sheep IgG deposition, mean fluorescence intensity was measured using ImageJ⁶⁷ (30 glomeruli/sample). The number of WT1⁺ cells found within or outside (in glomerular crescents or lining the Bowman's capsule) the glomerular tuft was counted in 50 consecutive glomeruli/sample. To account for any changes in glomerular tuft area, the number of WT1⁺ cells in the glomerular tuft was normalised to the glomerular area (measured using ImageJ⁶⁷) in 15 glomeruli/sample. Apoptosis was identified using TUNEL (Roche, Burgess Hill, UK). The number of TUNEL⁺ and WT1⁺/TUNEL⁺ cells was counted in 50 glomeruli/sample.

Measurement of murine IgG subclasses specific for sheep IgG

The titres of murine IgG subclasses specific for sheep IgG were measured by ELISA in plasma as described⁶⁸ using alkaline phosphatase subclass-specific antibodies for IgG1, IgG2b and IgG3 (SouthernBiotech, Birmingham, AL) and IgG2a (Bethyl Laboratories).

***In-situ* hybridisation**

In-situ hybridisation on paraffin sections was performed as described,²⁷ using a digoxigenin-labelled antisense riboprobe specific for the 3'UTR of *Tmsb4x*, alongside a sense control.

Electron microscopy

For transmission electron microscopy, kidney cortex specimens (1mm³) were post-fixed in osmium tetroxide, dehydrated in acetone, and embedded in epoxy resin. Ultrathin sections were stained with uranyl-acetate and lead citrate and examined.

Quantitative real-time PCR

RNA was extracted from mouse whole kidney or glomerular extracts (isolated by Dynabeads²⁸). 500ng was used to prepare cDNA (iScript kit, Bio-Rad, Hemel Hempstead, UK) and qRT-PCR performed as described²⁸ with *Hprt* as a housekeeping gene. All measurements were performed in duplicate. Renal biopsies from patients with RPGN (n=12), SLE (n=12) and LD controls (n=7) were collected within the framework of the European Renal cDNA Bank - Kroener–Fresenius Biopsy Bank⁶⁹ after informed consent and local ethical approval. Unfixed tissue was transferred to RNase inhibitor and manually micro-dissected into glomerular and tubulointerstitial compartments. Total RNA was isolated and qRT-PCR performed as reported⁶⁹ with 18S rRNA (Applied Biosystems) as the reference gene. Primer details are available on request.

Cell culture

Mouse podocytes³⁷ were cultured as described⁷⁰ and allowed to differentiate for 14 days. Cells were transfected with 10nM siRNA specific for *Tmsb4x* or with a non-targeting control (both from Santa Cruz Biotechnology, Dallas, TX) using the transfection reagent, Lipofectamine® RNAiMAX (Thermo Fisher Scientific) according to the manufacturer's instructions.

Cell viability was assessed 24, 48 and 72 hours post-transfection using the methyltetrazolium assay. To assess migration podocytes were plated to confluence and a scratch created using a pipette tip. Images (four fields/condition) were taken 0, 6 and 24 hours later and the number of cells that migrated into the wound area counted. To visualise F-actin filaments 48 hours post-transfection podocytes were fixed in 4% paraformaldehyde,

4% sucrose and stained with AlexaFluor-594 phalloidin (Thermo Fisher Scientific). The arrangement of actin filaments (either cytoplasmic stress fibres or cortical actin) was assessed in thirty cells/condition. RhoA and Cdc42 activity were quantified in podocyte lysates by G-LISA® Small G-protein Activation Assays (Cytoskeleton, Denver, CO).

Glomeruli from *Tmsb4x^{+y}* and *Tmsb4x^{-y}* mice were isolated by Dynabeads²⁸ and cultured in Matrigel-coated plates (Corning, Tewksbury, MA) in DMEM:F12 with 10% FCS, 1% ITS, 100µg/ml penicillin (Thermo Fisher Scientific). On day 7, when podocytes had grown out of the glomeruli, they were detached using trypsin-EDTA and separated from glomeruli using 40µm cell strainers (Corning). Primary podocytes obtained with this method were >90% pure as judged by cell morphology and staining using podocyte (nephrin, nestin) markers.

Statistical Methods

All samples were assessed blinded to treatment. Data is presented as means±SEM and was analysed using GraphPad Prism (GraphPad Software, La Jolla, CA). When differences between two groups were evaluated data was analysed by t-test. When three or more groups were assessed one-way ANOVA with Bonferroni's multiple comparison post-hoc tests was used. Data affected by two variables was analysed using two-way ANOVA with Bonferroni's multiple comparison post-hoc tests. Statistical significance was accepted at $p \leq 0.05$.

DISCLOSURE

The authors have no competing interests to declare

FIGURE LEGENDS

Figure 1. *Tmsb4x* expression in the mouse glomerulus.

(A) Quantification of thymosin- β 4 (*Tmsb4x*) mRNA levels in mouse adult spleen, liver, heart and kidney by qRT-PCR. *Tmsb4x* expression was also quantified in glomeruli-depleted [glom (-)] and glomeruli-enriched [glom (+)] kidney homogenates. The bars represent the mean of three samples \pm SEM. (B-C) *In situ* hybridisation for *Tmsb4x* on E16.5 mouse kidney sections. Cells positive for *Tmsb4x* are indicated by arrows. (D-F) Immunohistochemistry for *Tmsb4x* in the mouse glomerulus at E18 (D), 1 week (E) and 8 weeks of age (F). Cells positive for *Tmsb4x* are indicated by arrows. (G-I) Representative pictures for *Tmsb4x* (G) and nephrin (Nphs1) (H) staining in the mouse adult wild-type glomerulus visualised by fluorescent microscopy. (I) Merged image showing Nphs1 (red) and *Tmsb4x* (green) staining; areas of co-localisation are indicated by arrows. Scale bar = 20 μ m; **p \leq 0.01.

Figure 2. Renal function and glomerular morphology in *Tmsb4x*^{+/-} and *Tmsb4x*^{-/-} mice.

(A) Breeding scheme: Heterozygous female mice (*Tmsb4x*^{+/-}) were bred with hemizygous null male mice (*Tmsb4x*^{-/-}). Male wild-type (*Tmsb4x*^{+/+}) and *Tmsb4x*^{-/-} mice were compared in all subsequent experiments. (B) Twenty-four hour albumin excretion in urine of *Tmsb4x*^{+/-} (n=14-15) and *Tmsb4x*^{-/-} (n=9-10) mice collected at 1, 3, and 6 months of age. Data was log-transformed before analysis. (C) Blood urea nitrogen (BUN) concentration in *Tmsb4x*^{+/-} (n=9-15) and *Tmsb4x*^{-/-} mice (n=7-9) at 1, 3, and 6 months of age. Data was log-transformed before analysis. (D-E) Representative pictures of PAS staining of paraffin-embedded sections from *Tmsb4x*^{+/-} (D) and *Tmsb4x*^{-/-} (E) kidneys. Scale bar = 20 μ m. The glomerular score (F) was quantified as explained in the methods (*Tmsb4x*^{+/-}: n=4; *Tmsb4x*^{-/-}: n=5). (G-H) Representative images of the glomerular architecture of *Tmsb4x*^{+/-} (G) and *Tmsb4x*^{-/-} (H) kidneys assessed by transmission electron microscopy. An average of five glomeruli was examined per animal (*Tmsb4x*^{+/-}, n=4; *Tmsb4x*^{-/-}, n=3). (I-J) Representative pictures of

immunohistochemistry for thymosin- β 4 on paraffin-embedded sections from *Tmsb4x*^{+/-} (I) and *Tmsb4x*^{-/-} (J) kidneys from 6 month old mice. Thymosin- β 4-positive cells are indicated by arrows. Note: non-specific staining in tubules in *Tmsb4x*^{+/-} mice and *Tmsb4x*^{-/-} mice. Quantification of *Tmsb4x* (K), *Tmsb10* (L), *Tmsb15a* (M), *Tmsb15b* (N) and *Tmsb15l* (O) mRNA levels in whole kidney homogenates of *Tmsb4x*^{+/-} (n=8) and *Tmsb4x*^{-/-} (n=4) mice by qRT-PCR. Data is presented as mean \pm SEM. ***p \leq 0.001. Scale bar = 20 μ m.

Figure 3. Renal function in *Tmsb4x*^{+/-} and *Tmsb4x*^{-/-} mice following the induction of nephrotoxic nephritis.

(A) Outline of experimental strategy. Twenty-four hour albumin excretion in urine (B), urinary albumin to urinary creatinine ratio (C), plasma creatinine concentration (D), creatinine clearance (E) and blood urea nitrogen concentration (F) of *Tmsb4x*^{+/-} and *Tmsb4x*^{-/-} mice. Samples were collected prior to immunisation with Freund's adjuvant (*Tmsb4x*^{+/-}; control group) and 21 days after administration of nephrotoxic serum (*Tmsb4x*^{+/-} +NTS and *Tmsb4x*^{-/-} +NTS); n=12 for each group. Data was log-transformed before analysis and is presented as mean \pm SEM. (G) Glomerular score was quantified as described in the methods in *Tmsb4x*^{+/-} (n=5), *Tmsb4x*^{+/-} +NTS (n=9) and *Tmsb4x*^{-/-} +NTS (n=6) mice. Data is presented as mean \pm SEM. Representative pictures of PAS staining in glomeruli from control mice (*Tmsb4x*^{+/-}; H), and mice administered nephrotoxic serum (NTS) *Tmsb4x*^{+/-} +NTS (I) and *Tmsb4x*^{-/-} +NTS (J) are shown. Scale bar = 20 μ m. *p \leq 0.05, **p \leq 0.01, ***p \leq 0.001.

Figure 4. Podocyte assessment in *Tmsb4x*^{+/-} and *Tmsb4x*^{-/-} mice following the induction of nephrotoxic nephritis.

(A-C) Representative picture for nephrin (Nphs1; podocytes) (A) and *Tmsb4x* (B) staining in the mouse adult wild-type glomerulus 21 days after injection with nephrotoxic serum. Cells positive for both Nphs1 (green) and *Tmsb4x* (red) are indicated by arrows in the merged

picture **(C)**. **(D-F)** Representative pictures of glomeruli from *Tmsb4x*^{+/y} **(D)**, *Tmsb4x*^{+/y} +NTS **(E)** and *Tmsb4x*^{-/y} +NTS **(F)** mice stained for WT1. The glomerular tuft area is annotated by a dotted line. **(G-J)** Graphs showing the number of WT1-positive cells in the glomerular tuft **(G)**, the number of WT1-positive cells in the glomerular tuft normalised to glomerular area **(H)**, the number of WT1-positive cells in the area of the glomerulus surrounding the glomerular tuft **(I)** and the number of WT1-positive cells in the whole glomerulus **(J)**. Cells were counted in 50 glomeruli per sample, except for D, where cells were counted and normalised to the glomerular area in 15 glomeruli per sample. Data is presented as mean±SEM. *Tmsb4x*^{+/y} (n=5), *Tmsb4x*^{+/y} +NTS (n=9) and *Tmsb4x*^{-/y} +NTS (n=6) mice. Scale bar = 20µm.

Figure 5: Effects of downregulating endogenous *Tmsb4x* expression in podocytes *in vitro*.

(A) Podocytes grown *in vitro* under permissive conditions were differentiated for 14 days before transfecting them with control siRNA or siRNA targeting *Tmsb4x*. **(B)** Quantification of *Tmsb4x* mRNA levels in podocytes 48 hours after transfection. **(C)** Cell viability following knockdown of endogenous *Tmsb4x* was assessed by MTT assay. **(D)** Podocyte migration following knockdown of endogenous *Tmsb4x* was assessed by a wound-healing assay and the number of cells that migrated into the wound area was counted. **(E)** Representative pictures of podocytes transfected with control or *Tmsb4x* siRNA 0, 6 and 24 hours after wound formation. **(F-G)** Representative pictures showing a podocyte with cytoplasmic stress fibre F-actin distribution **(F)** or cortical F-actin distribution **(G)**. The percentage of cells with predominantly cytoplasmic stress fibres or cortical actin formation was quantified 48 hours after transfection **(H)**. **(I-J)** Quantification of active RhoA **(I)** and active Cdc42 **(J)** 48 hours after transfection. All experiments were repeated three to four times and the data is presented as mean±SEM. *p ≤ 0.05, ***p ≤ 0.001.

Figure 6. Assessment of inflammation in nephrotoxic nephritis.

(A-C) Representative picture for F4/80 (macrophages; **A**) and *Tmsb4x* staining (**B**). Cells positive for both F4/80 (green) and *Tmsb4x* (red) are shown in the merged picture (**C**) and are indicated by arrows. Images were taken by fluorescent microscopy. Scale bar = 20µm.

(D-F) Representative pictures showing Cd3 (T-cell marker) staining in the glomerular tuft (arrows) and in the peri-glomerular area (arrowheads) of *Tmsb4x*^{+/y} controls (**D**) and *Tmsb4x*^{+/y} (**E**) and *Tmsb4x*^{-/y} (**F**) mice 21 days following administration of nephrotoxic serum (NTS). The number of Cd3+ cells in the glomerular tuft (**G**) and in the peri-glomerular area (**H**) was counted in 50 glomeruli per sample and the average number was calculated (*Tmsb4x*^{+/y}, n=5, *Tmsb4x*^{+/y} +NTS, n=9, *Tmsb4x*^{-/y} +NTS, n=6). **(I-K)** Representative pictures showing F4/80 (activated macrophage marker) staining in the glomerular tuft (arrows) and the peri-glomerular area (arrowheads) of *Tmsb4x*^{+/y} controls (**I**) *Tmsb4x*^{+/y} +NTS (**J**) and *Tmsb4x*^{-/y} +NTS (**K**) mice. The number of F4/80+ cells in the glomerular tuft (**L**) and in the peri-glomerular area (**M**) was counted in 50 glomeruli per sample and the average number was calculated (*Tmsb4x*^{+/y}, n=5, *Tmsb4x*^{+/y} +NTS, n=8, *Tmsb4x*^{-/y} +NTS, n=6). Data is presented as mean±SEM. *p ≤ 0.05, **p ≤ 0.01, ***p ≤ 0.001. Scale bar = 20µm.

Figure 7. Assessment of fibrosis in nephrotoxic nephritis.

(A-C) Representative images showing collagen IV staining in glomeruli of *Tmsb4x*^{+/y} (**A**) *Tmsb4x*^{+/y} +NTS (**B**) and *Tmsb4x*^{-/y} +NTS (**C**) mice. **(N)** Quantification of collagen IV (*Col4a1*) mRNA levels in whole kidney homogenates of *Tmsb4x*^{+/y} (n=8), *Tmsb4x*^{+/y} +NTS (n=9) and *Tmsb4x*^{-/y} +NTS (n=6) mice. **(E-G)** Representative pictures showing alpha smooth muscle actin (α-SMA) staining in glomeruli of *Tmsb4x*^{+/y} (**E**) *Tmsb4x*^{+/y} +NTS (**F**) and *Tmsb4x*^{-/y} +NTS (**G**) mice. **(H)** Quantification of alpha smooth muscle actin (*Acta2*) mRNA levels in whole kidney homogenates of *Tmsb4x*^{+/y} (n=8), *Tmsb4x*^{+/y} +NTS (n=8) and *Tmsb4x*^{-/y}

^y+NTS (n=5) mice. Data is presented as mean±SEM. *p ≤ 0.05, **p ≤ 0.01. Scale bar = 20µm.

ACKNOWLEDGMENTS

We thank UCL Biological Services, Ms Hortensja Brzoska and Ms Sabrina Pacheco for their assistance with animal experiments and Professor Neil Dalton (King's College London) for creatinine measurements. This work was supported by a Kidney Research UK (KRUK) Senior Non-Clinical Fellowship (SF1/2008, to DAL), a KRUK Postdoctoral Fellowship (PDF8/2015 to EV), a Medical Research Council New Investigator Award (MR/J003638/1, to DAL) (MR/J003638/1) and by the National Institute for Health Research Biomedical Research Centre at Great Ormond Street Hospital for Children NHS Foundation Trust and University College London. CDC and MTL are supported by the Else Kröner Fresenius Foundation. We thank all participating centers of the European Renal cDNA Bank—Kroener–Fresenius Biopsy Bank (ERCB-KFB) and their patients for their cooperation. Active members at the time of the study are listed in ref. (Martini et al JASN 2014, Vol 25, No 11, 2559-2572).

REFERENCES

1. Eckardt KU, Coresh J, Devuyst O, *et al.* Evolving importance of kidney disease: from subspecialty to global health burden. *Lancet* 2013; 382: 158-169.
2. Greka A, Mundel P. Cell biology and pathology of podocytes. *Annu Rev Physiol* 2012; 74: 299-323.
3. Welsh GI, Saleem MA. The podocyte cytoskeleton--key to a functioning glomerulus in health and disease. *Nat Rev Nephrol* 2012; 8: 14-21.
4. Brinkkoetter PT, Ising C, Benzing T. The role of the podocyte in albumin filtration. *Nat Rev Nephrol* 2013; 9: 328-336.
5. Kurts C, Panzer U, Anders HJ, *et al.* The immune system and kidney disease: basic concepts and clinical implications. *Nat Rev Immunol* 2013; 13: 738-753.
6. Sanders MC, Goldstein AL, Wang YL. Thymosin beta 4 (Fx peptide) is a potent regulator of actin polymerization in living cells. *Proc Natl Acad Sci U S A* 1992; 89: 4678-4682.
7. Smart N, Bollini S, Dube KN, *et al.* De novo cardiomyocytes from within the activated adult heart after injury. *Nature* 2011; 474: 640-644.

8. Morris DC, Cui Y, Cheung WL, *et al.* A dose-response study of thymosin beta4 for the treatment of acute stroke. *J Neurol Sci* 2014; 345: 61-67.
9. Sosne G, Qiu P, Ousler GW, 3rd, *et al.* Thymosin beta4: a potential novel dry eye therapy. *Ann N Y Acad Sci* 2012; 1270: 45-50.
10. Conte E, Genovese T, Gili E, *et al.* Thymosin beta4 protects C57BL/6 mice from bleomycin-induced damage in the lung. *Eur J Clin Invest* 2013; 43: 309-315.
11. Goldstein AL, Hannappel E, Sosne G, *et al.* Thymosin beta4: a multi-functional regenerative peptide. Basic properties and clinical applications. *Expert Opin Biol Ther* 2012; 12: 37-51.
12. Fan Y, Gong Y, Ghosh PK, *et al.* Spatial coordination of actin polymerization and ILK-Akt2 activity during endothelial cell migration. *Dev Cell* 2009; 16: 661-674.
13. Santra M, Zhang ZG, Yang J, *et al.* Thymosin beta4 up-regulation of microRNA-146a promotes oligodendrocyte differentiation and suppression of the Toll-like proinflammatory pathway. *J Biol Chem* 2014; 289: 19508-19518.
14. Bock-Marquette I, Saxena A, White MD, *et al.* Thymosin beta4 activates integrin-linked kinase and promotes cardiac cell migration, survival and cardiac repair. *Nature* 2004; 432: 466-472.

15. Smart N, Risebro CA, Melville AA, *et al.* Thymosin beta4 induces adult epicardial progenitor mobilization and neovascularization. *Nature* 2007; 445: 177-182.
16. Sosne G, Qiu P, Christopherson PL, *et al.* Thymosin beta 4 suppression of corneal NFkappaB: a potential anti-inflammatory pathway. *Exp Eye Res* 2007; 84: 663-669.
17. Vasilopoulou E, Winyard PJ, Riley PR, *et al.* The role of thymosin-beta4 in kidney disease. *Expert Opin Biol Ther* 2015; 15 S187-190.
18. Zuo Y, Chun B, Potthoff SA, *et al.* Thymosin beta4 and its degradation product, Ac-SDKP, are novel reparative factors in renal fibrosis. *Kidney Int* 2013; 84: 1166-1175.
19. Zhu J, Su LP, Zhou Y, *et al.* Thymosin beta4 Attenuates Early Diabetic Nephropathy in a Mouse Model of Type 2 Diabetes Mellitus. *Am J Ther* 2015; 22: 141-146.
20. Cavasin MA, Rhaleb NE, Yang XP, *et al.* Prolyl oligopeptidase is involved in release of the antifibrotic peptide Ac-SDKP. *Hypertension* 2004; 43: 1140-1145.
21. Liao TD, Yang XP, D'Ambrosio M, *et al.* N-acetyl-seryl-aspartyl-lysyl-proline attenuates renal injury and dysfunction in hypertensive rats with reduced renal mass: council for high blood pressure research. *Hypertension* 2010; 55: 459-467.
22. Omata M, Taniguchi H, Koya D, *et al.* N-acetyl-seryl-aspartyl-lysyl-proline ameliorates the progression of renal dysfunction and fibrosis in WKY rats with

- established anti-glomerular basement membrane nephritis. *J Am Soc Nephrol* 2006; 17: 674-685.
23. Rhaleb NE, Pokharel S, Sharma U, *et al.* Renal protective effects of N-acetyl-Ser-Asp-Lys-Pro in deoxycorticosterone acetate-salt hypertensive mice. *J Hypertension* 2011; 29: 330-338.
 24. Guinobert I, Viltard M, Piquemal D, *et al.* Identification of differentially expressed genes between fetal and adult mouse kidney: candidate gene in kidney development. *Nephron Physiol* 2006; 102: p81-91.
 25. Brunskill EW, Georgas K, Rumballe B, *et al.* Defining the molecular character of the developing and adult kidney podocyte. *PLoS One* 2011; 6: e24640.
 26. Xu BJ, Shyr Y, Liang X, *et al.* Proteomic patterns and prediction of glomerulosclerosis and its mechanisms. *J Am Soc Nephrol* 2005; 16: 2967-2975.
 27. Rossdeutsch A, Smart N, Dube KN, *et al.* Essential Role for Thymosin beta4 in Regulating Vascular Smooth Muscle Cell Development and Vessel Wall Stability. *Circ Res* 2012; 111: e89-e102.
 28. Long DA, Kolatsi-Joannou M, Price KL, *et al.* Albuminuria is associated with too few glomeruli and too much testosterone. *Kidney Int* 2013; 83: 1118-1129.

29. Li X, Chuang PY, D'Agati VD, *et al.* Nephrin Preserves Podocyte Viability and Glomerular Structure and Function in Adult Kidneys. *J Am Soc Nephrol* 2015; 26: 2361-2377.
30. Thorner PS, Ho M, Eremina V, *et al.* Podocytes contribute to the formation of glomerular crescents. *J Am Soc Nephrol* 2008; 19: 495-502.
31. Li X, Zimmerman A, Copeland NG, *et al.* The mouse thymosin beta 4 gene: structure, promoter identification, and chromosome localization. *Genomics* 1996; 32: 388-394.
32. Pippin JW, Brinkkoetter PT, Cormack-Aboud FC, *et al.* Inducible rodent models of acquired podocyte diseases. *Am J Physiol Renal Physiol* 2009; 296: F213-229.
33. Khan SB, Cook HT, Bhangal G, *et al.* Antibody blockade of TNF-alpha reduces inflammation and scarring in experimental crescentic glomerulonephritis. *Kidney Int* 2005; 67: 1812-1820.
34. Le Hir M, Keller C, Eschmann V, *et al.* Podocyte bridges between the tuft and Bowman's capsule: an early event in experimental crescentic glomerulonephritis. *J Am Soc Nephrol* 2001; 12: 2060-2071.
35. Guo JK, Menke AL, Gubler MC, *et al.* WT1 is a key regulator of podocyte function: reduced expression levels cause crescentic glomerulonephritis and mesangial sclerosis. *Human Mol Genet* 2002; 11: 651-659.

36. Davis B, Dei Cas A, Long DA, *et al.* Podocyte-specific expression of angiopoietin-2 causes proteinuria and apoptosis of glomerular endothelia. *J Am Soc Nephrol* 2007; 18: 2320-2329.
37. Mundel P, Reiser J, Zuniga Mejia Borja A, *et al.* Rearrangements of the cytoskeleton and cell contacts induce process formation during differentiation of conditionally immortalized mouse podocyte cell lines. *Exp Cell Res* 1997; 236: 248-258.
38. Pollard TD, Cooper JA. Actin, a central player in cell shape and movement. *Science* 2009; 326: 1208-1212.
39. Raftopoulou M, Hall A. Cell migration: Rho GTPases lead the way. *Dev Biol* 2004; 265: 23-32.
40. Hannappel E, Xu GJ, Morgan J, *et al.* Thymosin beta 4: a ubiquitous peptide in rat and mouse tissues. *Proc Natl Acad Sci U S A* 1982; 79: 2172-2175.
41. Peng H, Xu J, Yang XP, *et al.* Thymosin-beta4 prevents cardiac rupture and improves cardiac function in mice with myocardial infarction. *Am J Physiol Heart Circ Physiol* 2014; 307: H741-751.
42. Duffield JS, Tipping PG, Kipari T, *et al.* Conditional ablation of macrophages halts progression of crescentic glomerulonephritis. *Am J Pathol* 2005; 167: 1207-1219.

43. Huang XR, Tipping PG, Apostolopoulos J, *et al.* Mechanisms of T cell-induced glomerular injury in anti-glomerular basement membrane (GBM) glomerulonephritis in rats. *Clin Exp Immunol* 1997; 109: 134-142.
44. Tipping PG, Huang XR, Qi M, *et al.* Crescentic glomerulonephritis in CD4- and CD8-deficient mice. Requirement for CD4 but not CD8 cells. *Am J Pathol* 1998; 152: 1541-1548.
45. Nemolato S, Cabras T, Fanari MU, *et al.* Immunoreactivity of thymosin beta 4 in human foetal and adult genitourinary tract. *Eur J Histochem* 2010; 54: e43.
46. Knop J, App C, Hannappel E. Antibodies in research of thymosin beta4: investigation of cross-reactivity and influence of fixatives. *Ann N Y Acad Sci* 2012; 1270: 105-111.
47. Bravo-Cordero JJ, Magalhaes MA, Eddy RJ, *et al.* Functions of cofilin in cell locomotion and invasion. *Nat Rev Mol Cell Biol* 2013; 14: 405-415.
48. Moeller MJ, Soofi A, Hartmann I, *et al.* Podocytes populate cellular crescents in a murine model of inflammatory glomerulonephritis. *J Am Soc Nephrol* 2004; 15: 61-67.
49. Asanuma K, Yanagida-Asanuma E, Faul C, *et al.* Synaptopodin orchestrates actin organization and cell motility via regulation of RhoA signalling. *Nat Cell Biol* 2006; 8: 485-491.

50. Wang L, Ellis MJ, Gomez JA, *et al.* Mechanisms of the proteinuria induced by Rho GTPases. *Kidney Int* 2012; 81: 1075-1085.
51. Zhu L, Jiang R, Aoudjit L, *et al.* Activation of RhoA in podocytes induces focal segmental glomerulosclerosis. *J Am Soc Nephrol* 2011; 22: 1621-1630.
52. Babelova A, Jansen F, Sander K, *et al.* Activation of Rac-1 and RhoA contributes to podocyte injury in chronic kidney disease. *PLoS One* 2013; 8: e80328.
53. Hidaka T, Suzuki Y, Yamashita M, *et al.* Amelioration of crescentic glomerulonephritis by RhoA kinase inhibitor, Fasudil, through podocyte protection and prevention of leukocyte migration. *Am J Pathol* 2008; 172: 603-614.
54. Tian D, Jacobo SM, Billing D, *et al.* Antagonistic regulation of actin dynamics and cell motility by TRPC5 and TRPC6 channels. *Sci Signal* 2010; 3: ra77.
55. Ridley AJ. Rho GTPase signalling in cell migration. *Curr Opin Cell Biol* 2015; 36: 103-112.
56. Gee HY, Saisawat P, Ashraf S, *et al.* ARHGDI1 mutations cause nephrotic syndrome via defective RHO GTPase signaling. *J Clin Invest* 2013; 123: 3243-3253.
57. McWhorter FY, Wang T, Nguyen P, *et al.* Modulation of macrophage phenotype by cell shape. *Proc Natl Acad Sci U S A* 2013; 110: 17253-17258.

58. Man SM, Ekpenyong A, Tourlomousis P, *et al.* Actin polymerization as a key innate immune effector mechanism to control Salmonella infection. *Proc Natl Acad Sci U S A* 2014; 111: 17588-17593.
59. Evans MA, Smart N, Dube KN, *et al.* Thymosin beta4-sulfoxide attenuates inflammatory cell infiltration and promotes cardiac wound healing. *Nat Commun* 2013; 4: 2081.
60. Feng L, Tang WW, Loskutoff DJ, *et al.* Dysfunction of glomerular fibrinolysis in experimental antiglomerular basement membrane antibody glomerulonephritis. *J Am Soc Nephrol* 1993; 3: 1753-1764.
61. Huang XR, Chung AC, Zhou L, *et al.* Latent TGF-beta1 protects against crescentic glomerulonephritis. *J Am Soc Nephrol* 2008; 19: 233-242.
62. Brown HJ, Lock HR, Sacks SH, *et al.* TLR2 stimulation of intrinsic renal cells in the induction of immune-mediated glomerulonephritis. *J Immunol* 2006; 177: 1925-1931.
63. Dessapt-Baradez C, Woolf AS, White KE, *et al.* Targeted glomerular angiotensin-1 therapy for early diabetic kidney disease. *J Am Soc Nephrol* 2014; 25: 33-42.
64. Greenberg N, Roberts WL, Bachmann LM, *et al.* Specificity characteristics of 7 commercial creatinine measurement procedures by enzymatic and Jaffe method principles. *Clin Chem* 2012; 58: 391-401.

65. Kolatsi-Joannou M, Price KL, Winyard PJ, *et al.* Modified citrus pectin reduces galectin-3 expression and disease severity in experimental acute kidney injury. *PLoS One* 2011; 6: e18683.
66. Huang JL, Woolf AS, Kolatsi-Joannou M, *et al.* Vascular Endothelial Growth Factor C for Polycystic Kidney Diseases. *J Am Soc Nephrol* 2016; 27: 69-77.
67. Schneider CA, Rasband WS, Eliceiri KW. NIH Image to ImageJ: 25 years of image analysis. *Nat Methods* 2012; 9: 671-675.
68. Brown HJ, Sacks SH, Robson MG. Toll-like receptor 2 agonists exacerbate accelerated nephrotoxic nephritis. *J Am Soc Nephrol* 2006; 17: 1931-1939.
69. Cohen CD, Frach K, Schlondorff D, *et al.* Quantitative gene expression analysis in renal biopsies: a novel protocol for a high-throughput multicenter application. *Kidney Int* 2002; 61: 133-140.
70. Yates LL, Papakrivopoulou J, Long DA, *et al.* The planar cell polarity gene Vangl2 is required for mammalian kidney-branching morphogenesis and glomerular maturation. *Human Mol Genet* 2010; 19: 4663-4676.

Figure 1

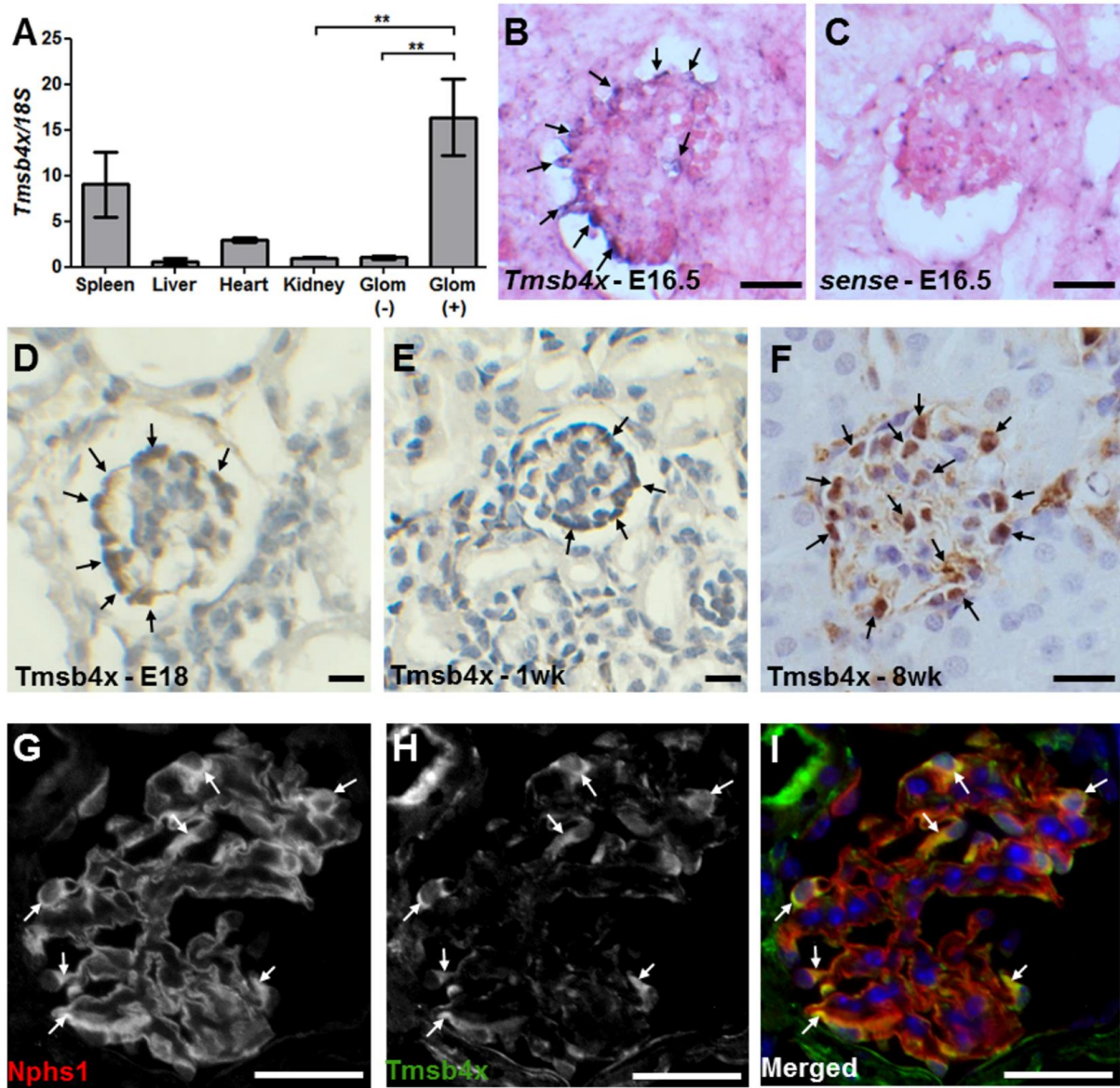


Figure 2

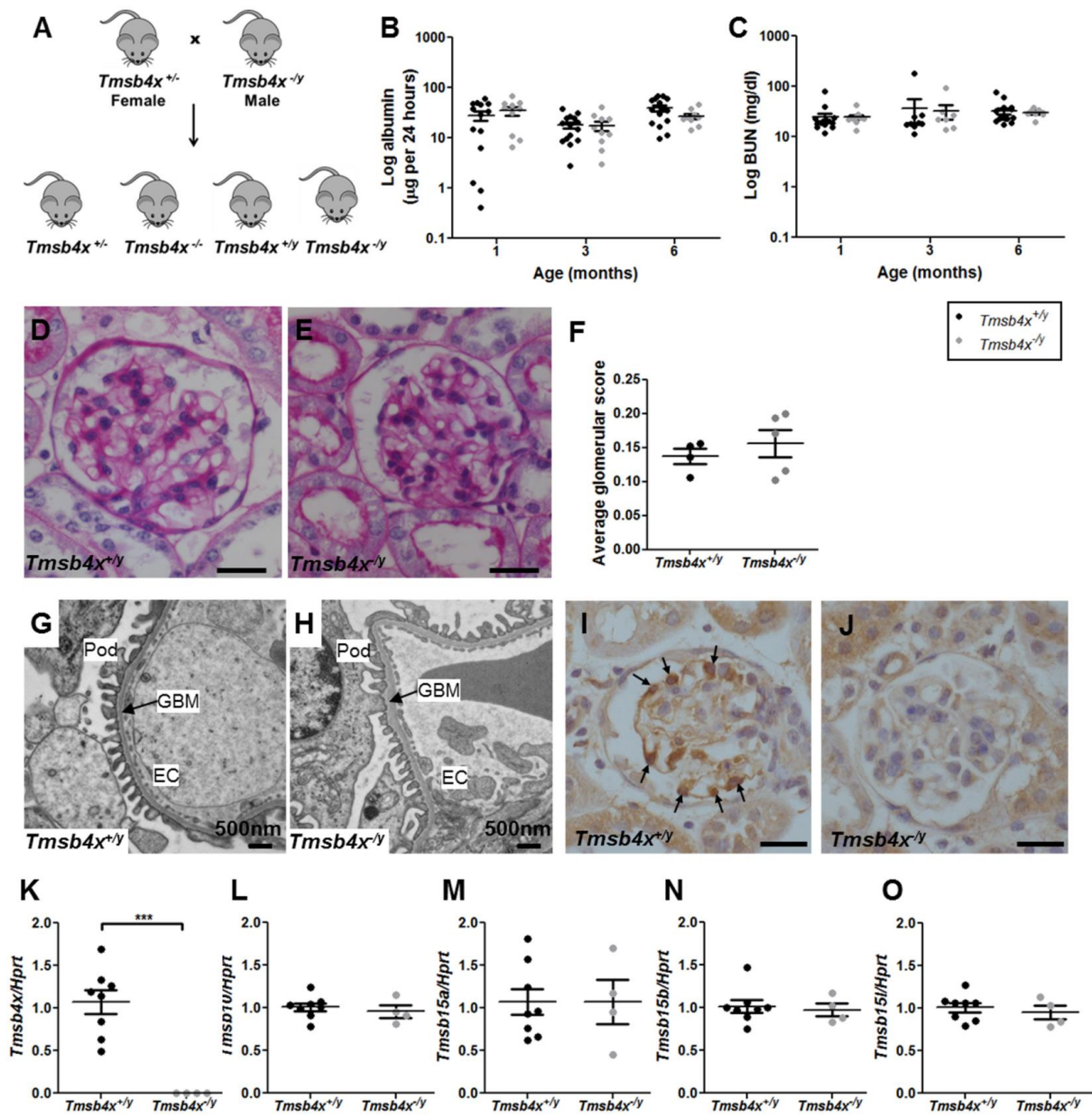


Figure 3

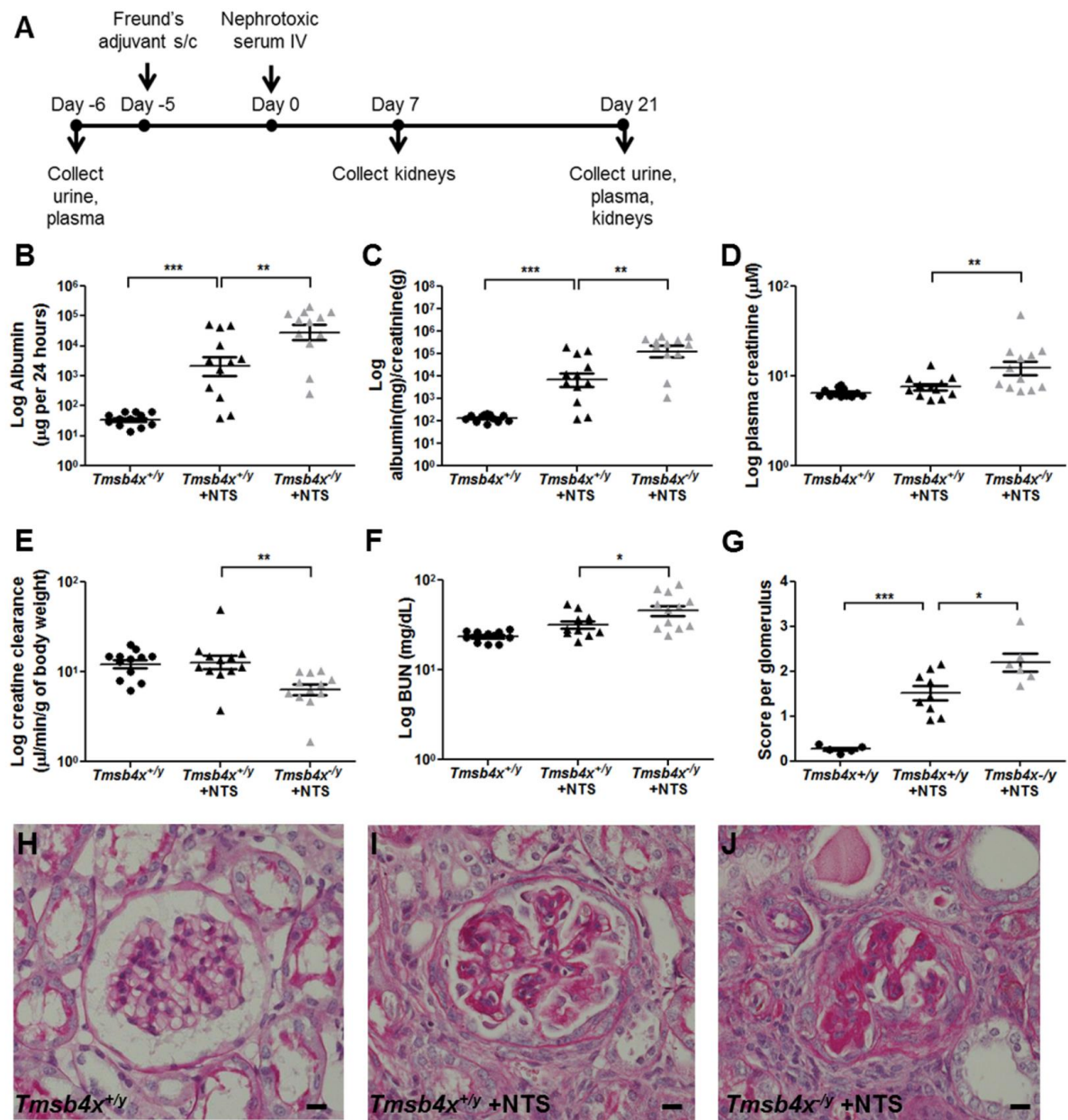


Figure 4

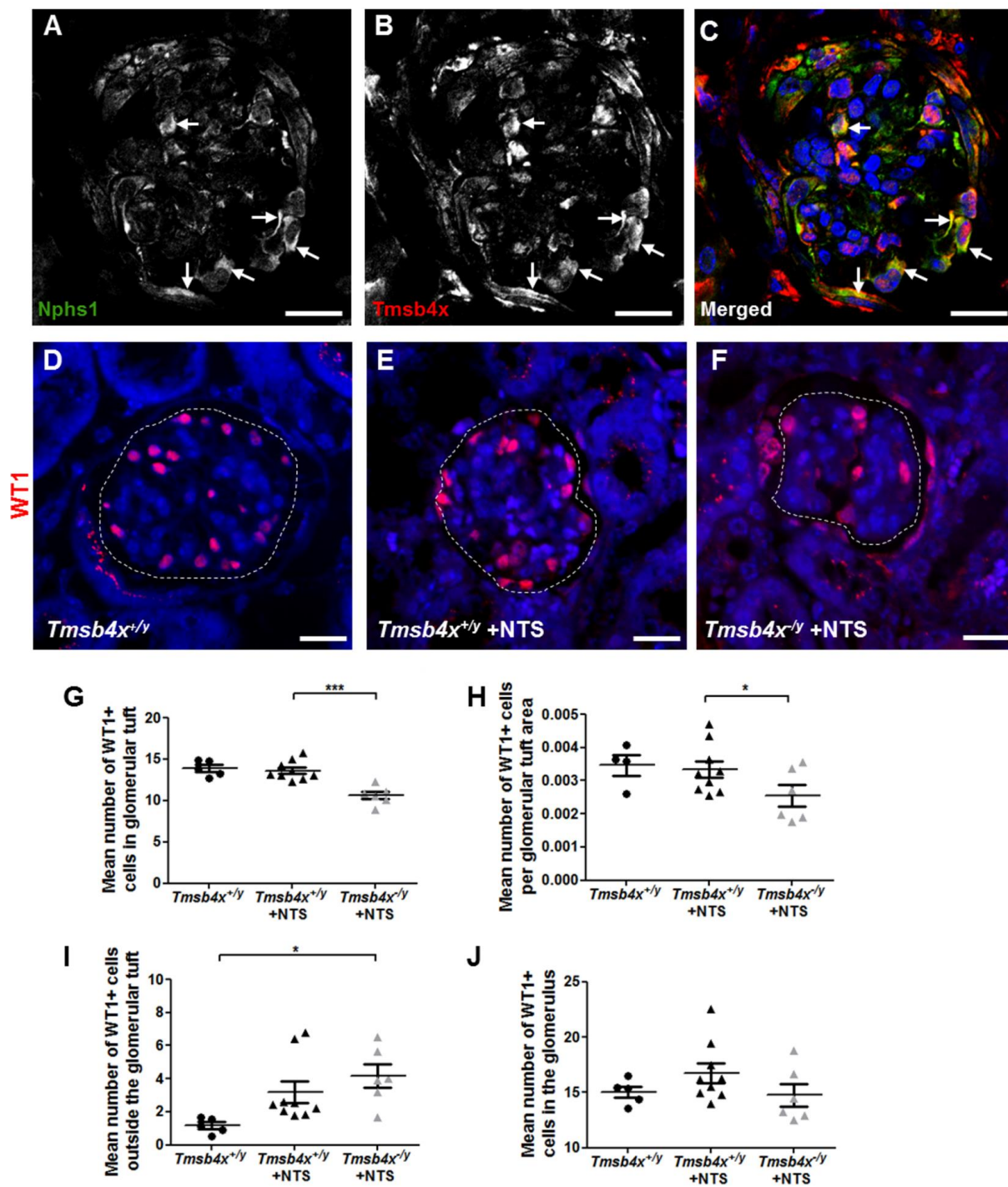


Figure 5

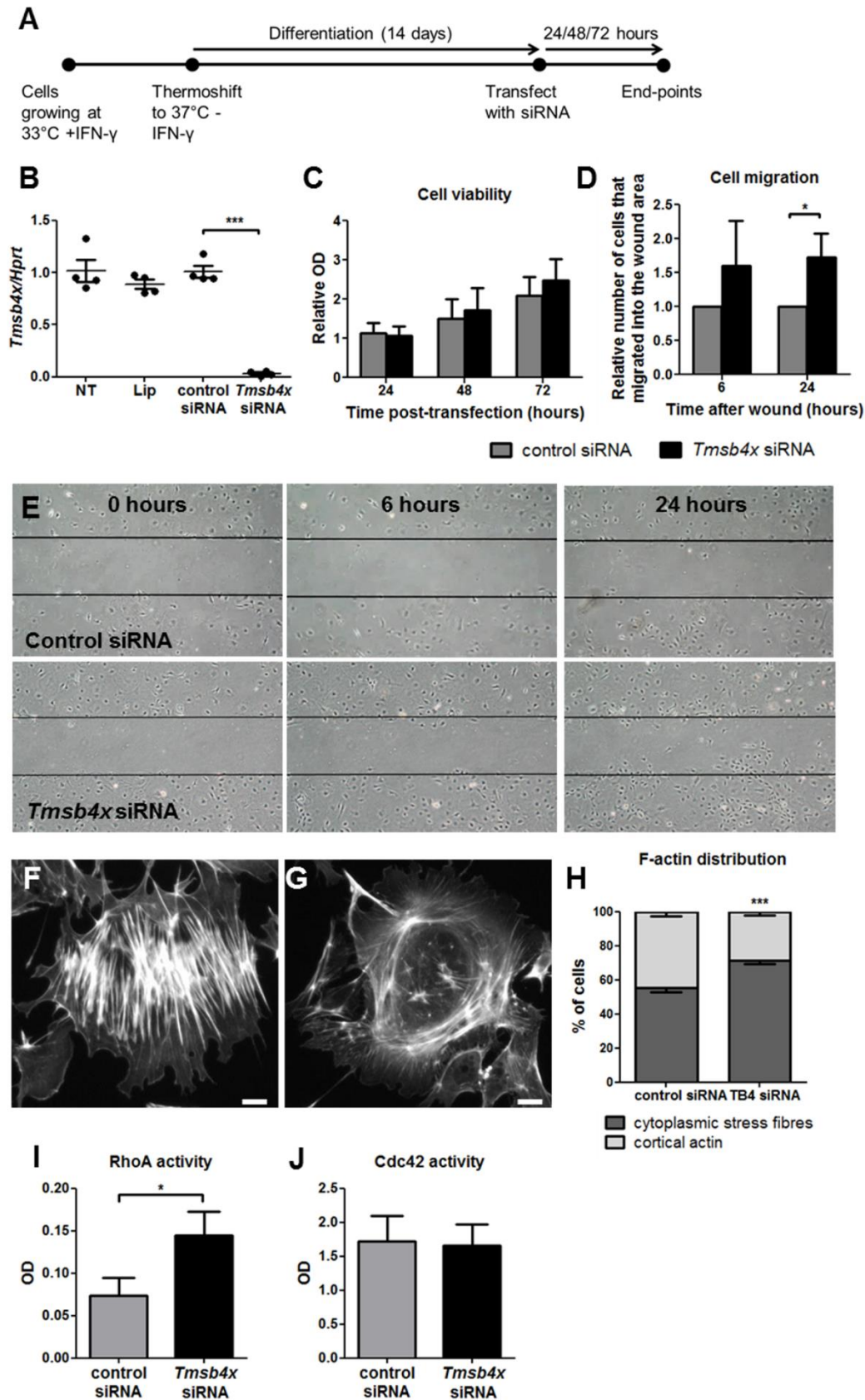


Figure 6

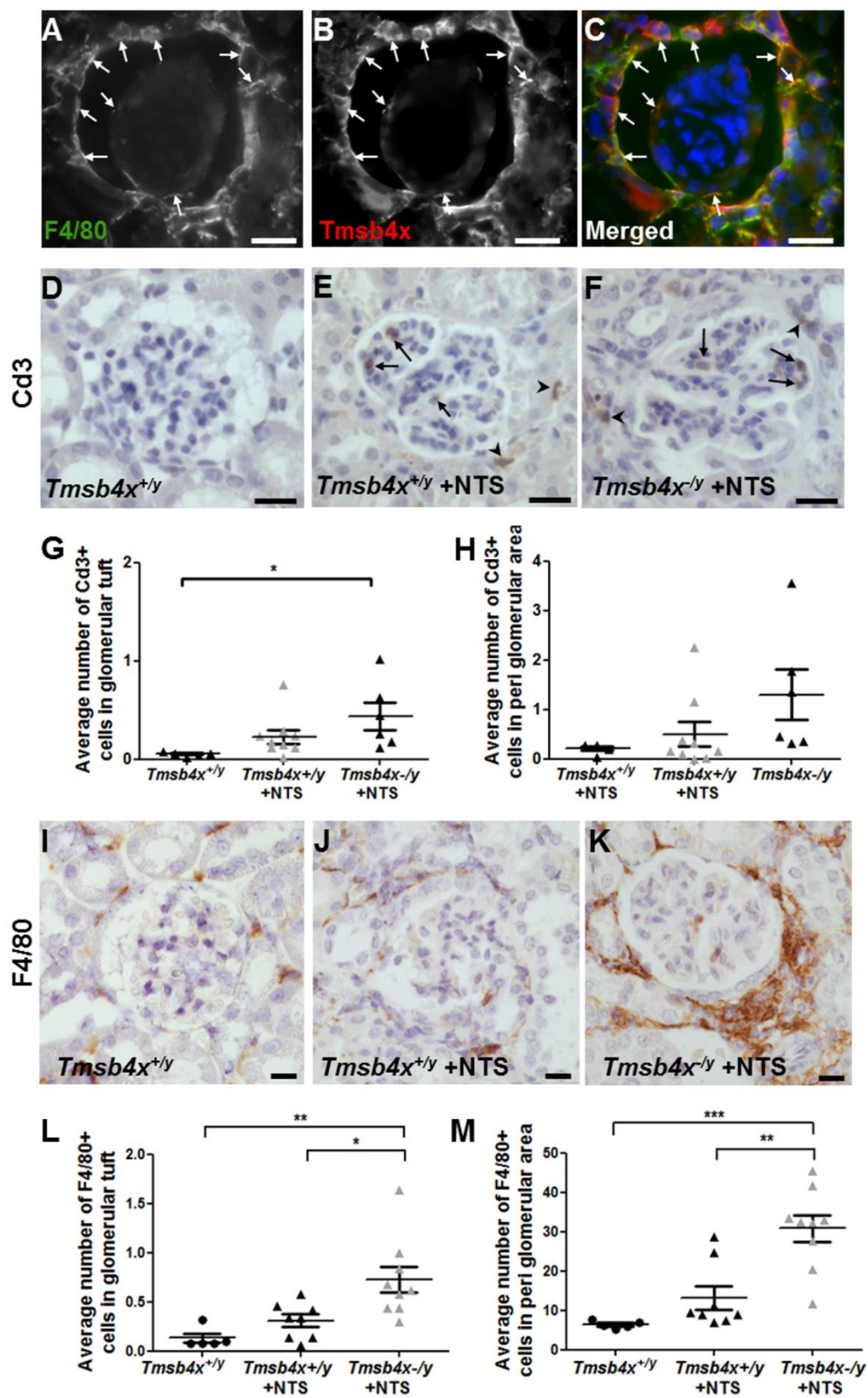
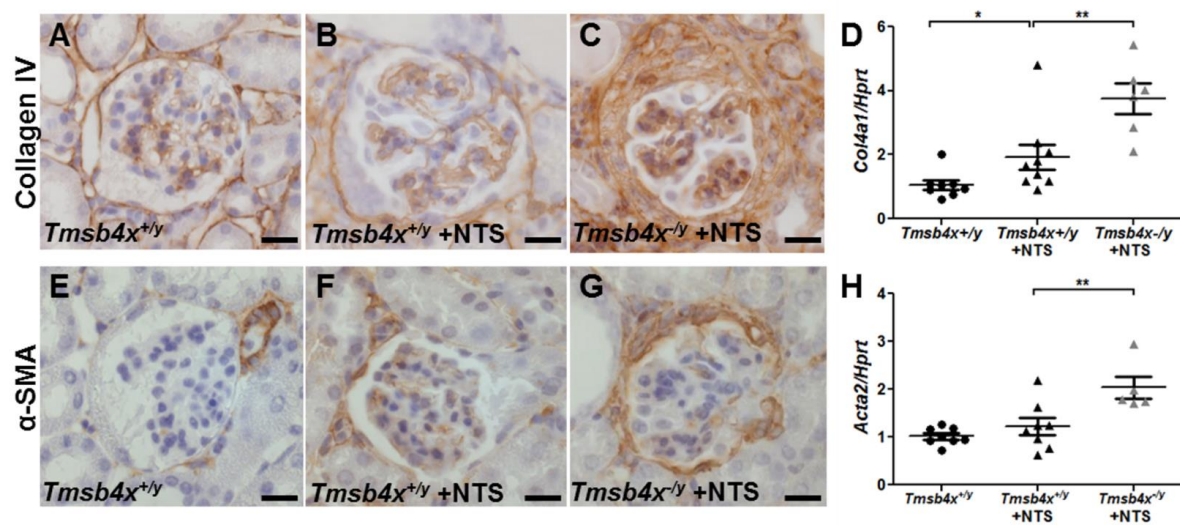


Figure 7



Supplementary Data

Loss of endogenous thymosin- β 4 accelerates glomerular disease

Elisavet Vasilopoulou¹, Maria Kolatsi-Joannou¹, Maja T Lindenmeyer², Kathryn E White³, Michael G Robson⁴, Clemens D Cohen², Neil J Sebire¹, Paul R Riley⁵, Paul J Winyard¹, David A Long¹

¹Developmental Biology and Cancer Programme, UCL Institute of Child Health, London, WC1N 1EH, UK.

²Nephrological Center, Medical Clinic and Policlinic IV, University of Munich, Munich, Germany

³EM Research Services, University of Newcastle, Newcastle upon Tyne, NE2 4HH, UK

⁴MRC Centre for Transplantation, King's College London, London, SE1 9RT, UK

⁵Department of Physiology, Anatomy and Genetics, University of Oxford, Oxford, OX1 3PT, UK

Corresponding Author

David A Long PhD, Developmental Biology and Cancer Programme,
UCL Institute of Child Health, 30 Guilford Street, London, WC1N 1EH, UK.

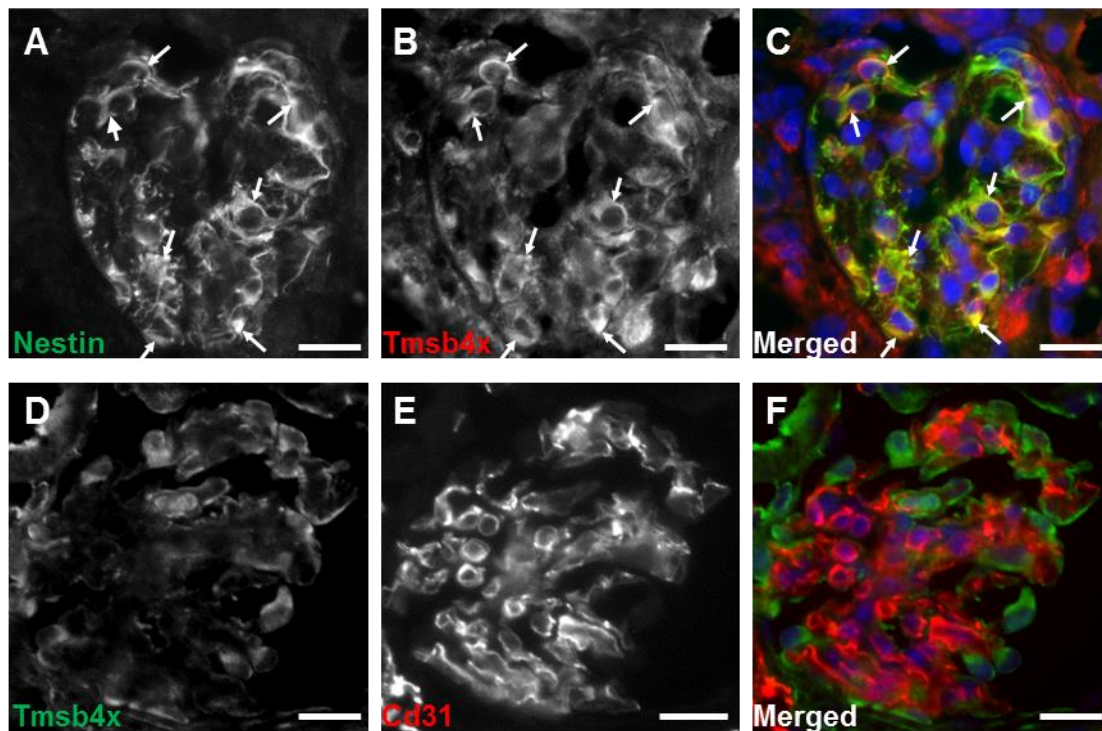
Tel: +44 (0)207 905 2615

Fax: +44 (0)207 905 2133;

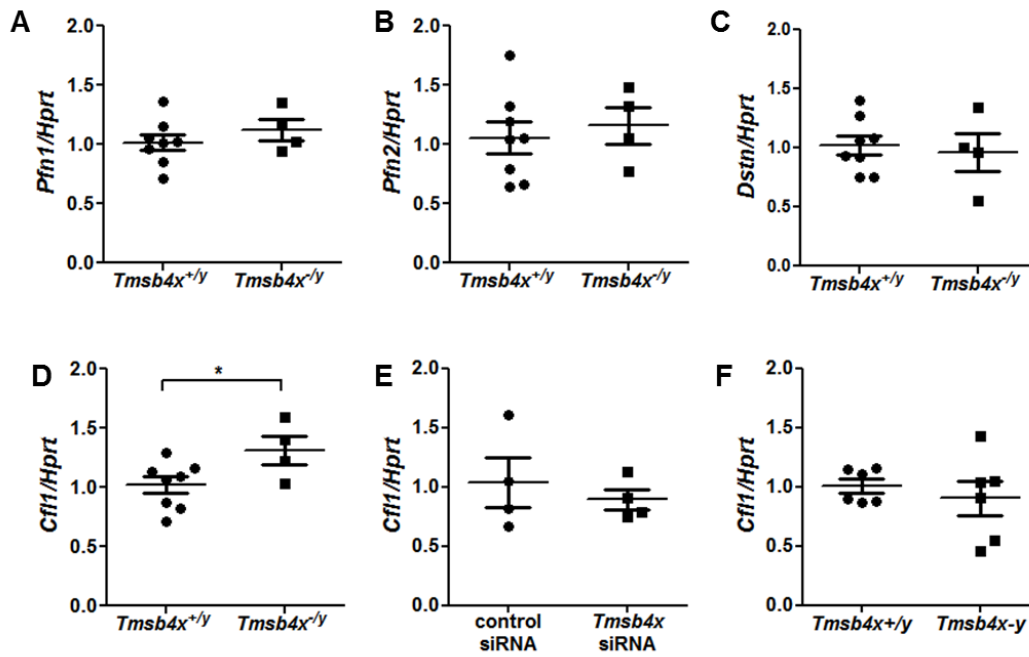
E-mail: d.long@ucl.ac.uk

Supplementary Table 1 Proportions of *Tmsb4x^{+/-}*, *Tmsb4x^{-/-}*, *Tmsb4x^{+y}* and *Tmsb4x^{-y}* mice born after crossing adult male *Tmsb4x^{-y}* mice with *Tmsb4x^{+/-}* adult females.

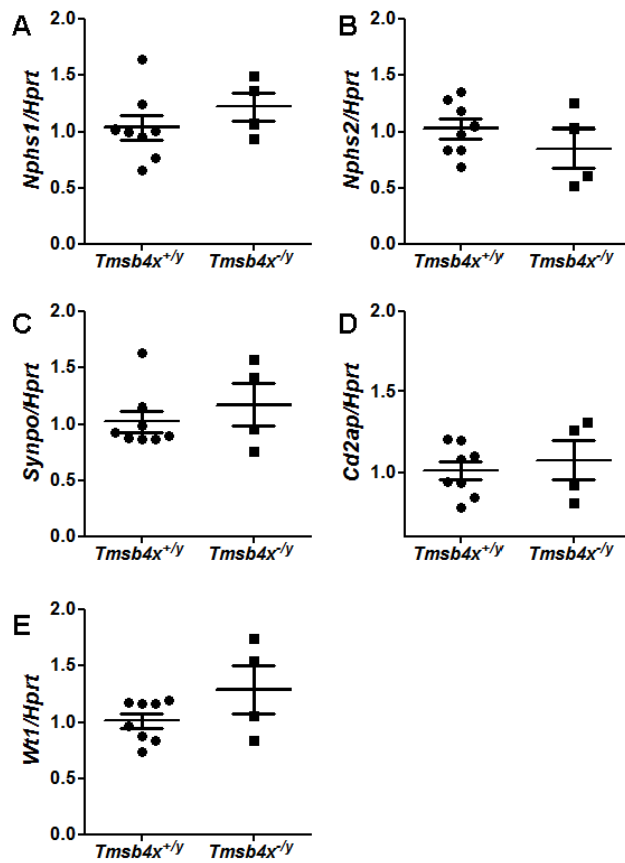
Genotype	<i>Tmsb4x^{+/-}</i>	<i>Tmsb4x^{-/-}</i>	<i>Tmsb4x^{+y}</i>	<i>Tmsb4x^{-y}</i>	Total	χ^2	P value
Expected	25%	25%	25%	25%			
Observed	92 (28%)	74 (23%)	85 (26%)	76 (23%)	327	2.554	0.4657



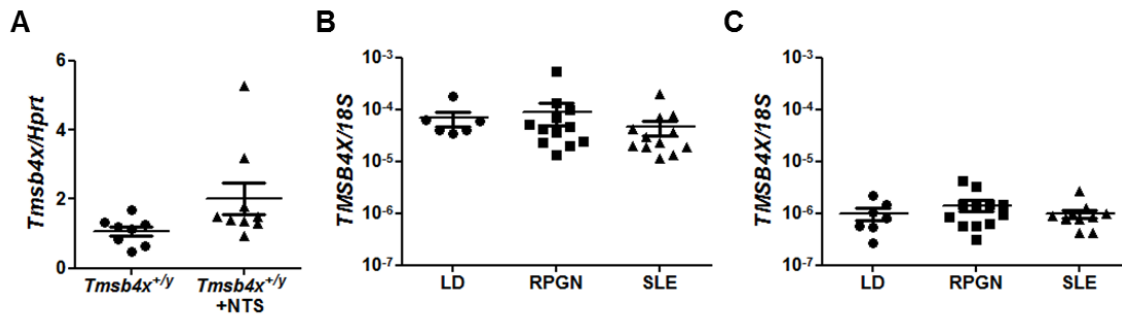
Supplementary Figure 1. (A-C) Representative pictures for Nestin (A) and Tmsb4x (B) staining in the mouse adult wild-type glomerulus visualised by fluorescent microscopy. (C) Merged image showing Tmsb4x (red) and Nestin (green) staining; areas of co-localisation are indicated by arrows. (D-F) Representative pictures for Tmsb4x (D) and Cd31 (E) staining in the mouse adult wild-type glomerulus visualised by fluorescent microscopy. (F) Merged image showing Tmsb4x (green) and Cd31 (red) staining. Scale bar = 20µm.



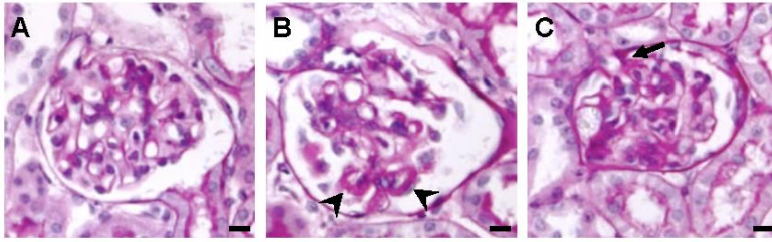
Supplementary Figure 2. Quantification of profilin 1 (*Pfn1*; **A**), profilin 2 (*Pfn2*; **B**), destrin (*Dstn*; **C**) and cofilin 1 (*Cfl1*; **D**) mRNA in whole kidney homogenates of *Tmsb4x^{+y}* (n=8) and *Tmsb4x^{-y}* (n=4) mice by qRT-PCR. Quantification of cofilin 1 (*Cfl1*) mRNA in podocytes 48 hours after transfection with control siRNA or siRNA targeting *Tmsb4x* (**E**, n=4) and in podocytes isolated from *Tmsb4x^{+y}* or *Tmsb4x^{-y}* mice (**F**, n=6). Data is presented as mean±SEM. *p<0.05



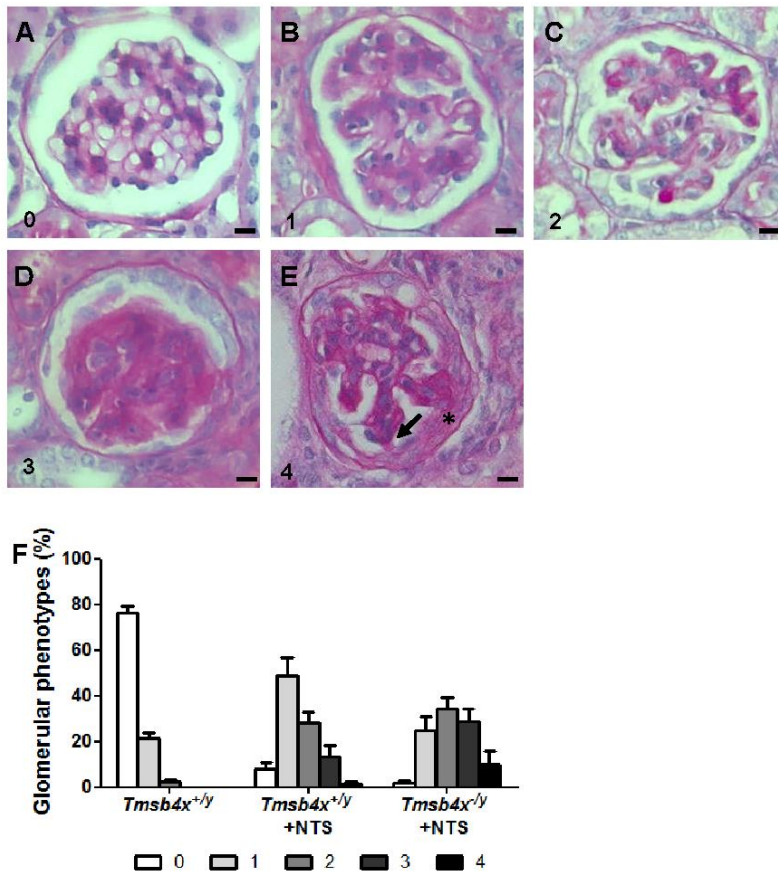
Supplementary Figure 3. Quantification of nephrin (*Nphp1*; **A**), podocin (*Nphp2*; **B**), synaptopodin (*Synpo*; **C**), cd2 associated protein (*Cd2ap*; **D**) and wilms tumor 1 (*Wt1*; **E**) mRNA in whole kidney homogenates of *Tmsb4x*^{+y} (n=8) and *Tmsb4x*^{-y} (n=4) mice by qRT-PCR. Data is presented as mean±SEM.



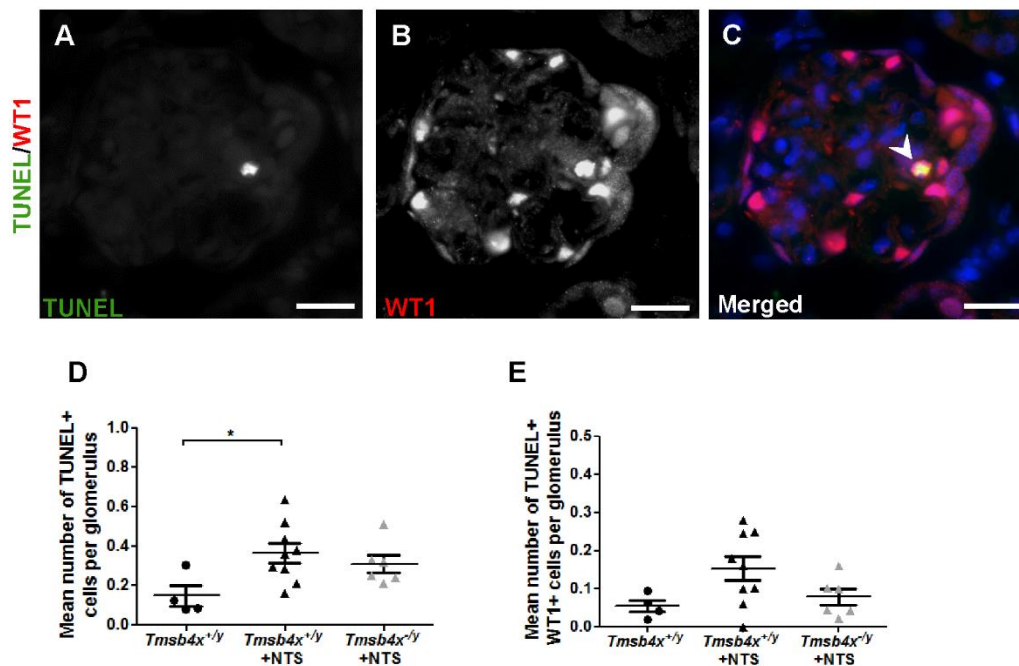
Supplementary Figure 4. (A) Quantification of *Tmsb4x* mRNA levels in whole kidney homogenates of *Tmsb4x*^{+/-y} (n=8) and *Tmsb4x*^{+/-y} +NTS (n=9) mice by qRT-PCR. (B-C) Quantification of *TMSB4X* mRNA levels in homogenates from human glomeruli (B) or tubulointerstitium (C). LD, living donor; RPGN, rapidly progressive glomerulonephritis; SLE, Lupus nephritis. Data is presented as mean±SEM.



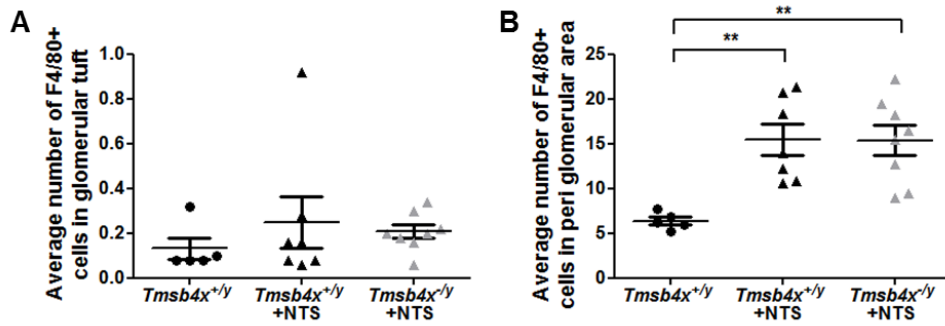
Supplementary Figure 5. Representative pictures of the histology observed 7 days after NTS administration showing a normal glomerulus **(A)**, a glomerulus with hyaline deposits indicated by arrowheads **(B)** and a glomerulus with a bridge formed between the tuft and Bowman's capsule indicated by an arrow **(C)**. Scale bar = 20 μ m.



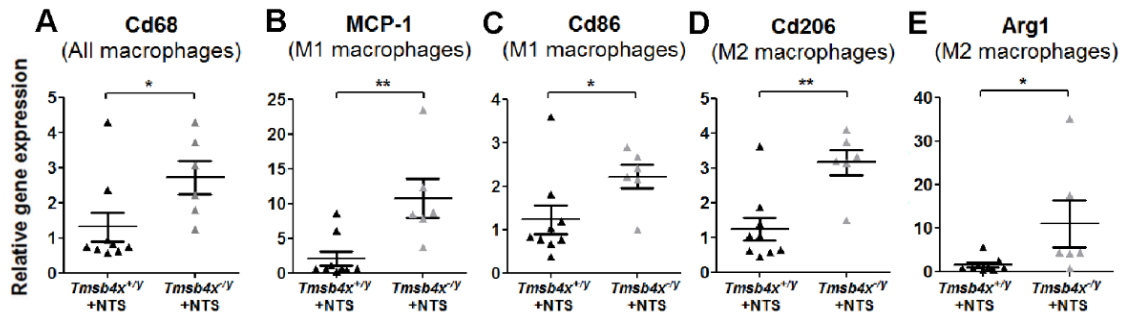
Supplementary Figure 6. (A-C) Representative pictures for the different scoring categories for glomerular injury showing (A) a normal glomerulus, score 0; (B) a glomerulus with increased mesangial matrix deposition and some loss of capillary loops, score 1; (C) a glomerulus with increased mesangial matrix deposition and focal areas of sclerosis, score 2; (D) a glomerulus with >50% sclerotic area and very few capillary loops, score 3 and (E) a sclerotic glomerulus with an epithelial hyperplastic lesion (*) and a bridge formed between the tuft and Bowman's capsule indicated by an arrow, score 4. Scale bar = 20 μ m. (F) Proportions of glomeruli in the different scoring categories of glomerular injury in *Tmsb4x^{+/y}* (n=5), *Tmsb4x^{+/y} +NTS* (n=9) and *Tmsb4x^{-/y} +NTS* (n=6) mice. Bars represent the mean \pm SEM.



Supplementary Figure 8. (A-C) Representative picture showing staining for TUNEL and WT1 in the glomerulus. A TUNEL-positive podocyte is identified by an arrowhead (**C**). The number of TUNEL-positive cells (**D**) and TUNEL-positive WT-1 positive cells per glomerulus was counted in 50 glomeruli per sample and the average number was calculated (*Tmsb4x*^{+/-}, n=4; *Tmsb4x*^{+/-} +NTS, n=9, *Tmsb4x*^{-/-} +NTS, n=6). Data is presented as mean±SEM. Scale bar = 20µm, *p ≤ 0.05.



Supplementary Figure 9. The number of F4/80+ cells in the glomerular tuft (**A**) and in the peri-glomerular area (**B**) 7 days following administration of nephrotoxic serum (NTS) was counted in 50 glomeruli per sample and the average number was calculated ($Tmsb4x^{+/y}$, n=5, $Tmsb4x^{+/y} + NTS$, n=6, $Tmsb4x^{-/y} + NTS$, n=8). Data is presented as mean \pm SEM. ** $p \leq 0.01$.



Supplementary Figure 10. Quantification of Cd68 (A), MCP-1 (B), Cd86 (C), Cd206 (D) and Arg1 (E) mRNA in whole kidney homogenates of *Tmsb4x*^{+/*y*} +NTS (n=9) and *Tmsb4x*^{-/*y*} +NTS (n=6) mice.